Quaternary Science Reviews 187 (2018) 177–202

Contents lists available at ScienceDirect

Quaternary Science Reviews

journal homepage: www.elsevier.com/locate/quascirev

Timing and nature of Holocene glacier advances at the northwestern end of the Himalayan-Tibetan orogen

Sourav Saha [a, *], Lewis A. Owen [a], Elizabeth N. Orr [a], Marc W. Caffee [b]

[a] Department of Geology, University of Cincinnati, Cincinnati, OH 45221, USA
[b] Department of Physics, Department of Earth, Atmospheric and Planetary Sciences, Purdue University, West Lafayette, IN 47907, USA

ARTICLE INFO

Article history:
Received 6 September 2017
Received in revised form
20 February 2018
Accepted 5 March 2018
Available online 30 March 2018

Keywords:
Holocene
Glaciation
Glacial geology
Cosmogenic surface exposure dating
Himalaya
Intertropical convergence zone
Paleoclimate

ABSTRACT

Holocene glacial chronostratigraphies are developed for four glaciated valleys at the northwestern end of the Himalayan-Tibetan orogen using geomorphic mapping and cosmogenic ^{10}Be surface exposure dating. The study areas include the Hamtah valley in the Lahul Himalaya, and the Karzok, Lato and upper Stok valleys in Zanskar. Five local glacial stages are dated to ~10.4, ~6.1–3.3, ~2.1–0.9, ~0.7–0.4, and ~0.3–0.2 ka based on 49 new moraine boulder ages. Large age dispersions are evident for each of the local glacial stages. This is especially the case for ~6.1–3.3 and ~2.1–0.9 ka, which is likely a result of prior and/or incomplete exposures in very young moraine boulders. An additional compilation of 187 published ^{10}Be moraine boulder ages help define seven Himalayan Holocene regional glacial stages (HHs) for the northwestern end of the Himalayan-Tibetan orogen. These HHs date to ~10.9–9.3, ~8.2–7.4, ~6.9–4.3, ~4.5–2.8, ~2.7–1.8, ~1.8–0.9, and <1 ka. Early Holocene glacier advances were generally more extensive and had larger equilibrium-line altitude depressions (ΔELA = ~425 ± 229 m) than glacier advances during the mid-Holocene (ΔELA = ~141 ± 106) and late Holocene (ΔELA = ~124 ± 121 m). The early Holocene glacier advances likely correspond to orbitally-forced northerly migration of the Intertropical Convergence Zone and enhanced summer monsoon. The timing of the majority of HHs during mid- and late Holocene corresponds well with the North Atlantic cooling that is likely teleconnected via mid-latitude westerlies, particularly during ~8 ka and after ~5 ka. These chronostratigraphies suggest that Holocene glaciation in the northwestern part of the Himalayan-Tibetan orogen is largely influenced by long-term orbital forcing amplified by large-scale migration of the Earth's thermal equator and the associated hemispheric oceanic-atmospheric systems.

1. Introduction

Over the past decade, several compilations of young glacial chronologies have been used to help reconstruct and understand the nature of Holocene glaciation on a global scale (Grove, 2008; Davis et al., 2009; Solomina et al., 2015, 2016). Most of these studies conclude that glacier advances during the Holocene in extratropical regions are broadly the consequence of climatic change driven by long-term orbital forcing, with occasional forcing by explosive volcanic eruptions and El Niño-Southern Oscillations (Solomina et al., 2015). Changes in oceanic-atmospheric circulations in the North Atlantic (Denton and Broecker, 2008; Chiang and Friedman, 2012, 2014; Wanner et al., 2015) represent another possible amplification mechanism. By way of contrast, long-term forcing behind Holocene glacier variability in the Himalaya has been attributed to distinct regional teleconnections, and do not correlate directly with orbital forcing (Solomina et al., 2015, 2016). Despite the impressive preservation of glacial landform assemblages throughout the Himalaya, this view has not been adequately tested due to the lack of well-defined Holocene glacial chronostratigraphies (Fig. 1A).

To examine the nature of Holocene glaciations and possible forcing factors behind glacier advances in the Himalaya, we developed Holocene glacial chronostratigraphies for four glaciated valleys at the northwestern end of the Himalayan-Tibetan orogen using remote sensing and field mapping, geomorphic techniques, and cosmic-ray-produced (cosmogenic) ^{10}Be surface exposure age dating. We also compare these new studies with existing glacial chronostratigraphies developed using ^{10}Be dating in adjacent

* Corresponding author. 500, Geology-Physics, University of Cincinnati, Cincinnati, Oh 45221, USA.
E-mail address: sahasv@mail.uc.edu (S. Saha).

https://doi.org/10.1016/j.quascirev.2018.03.009
0277-3791/

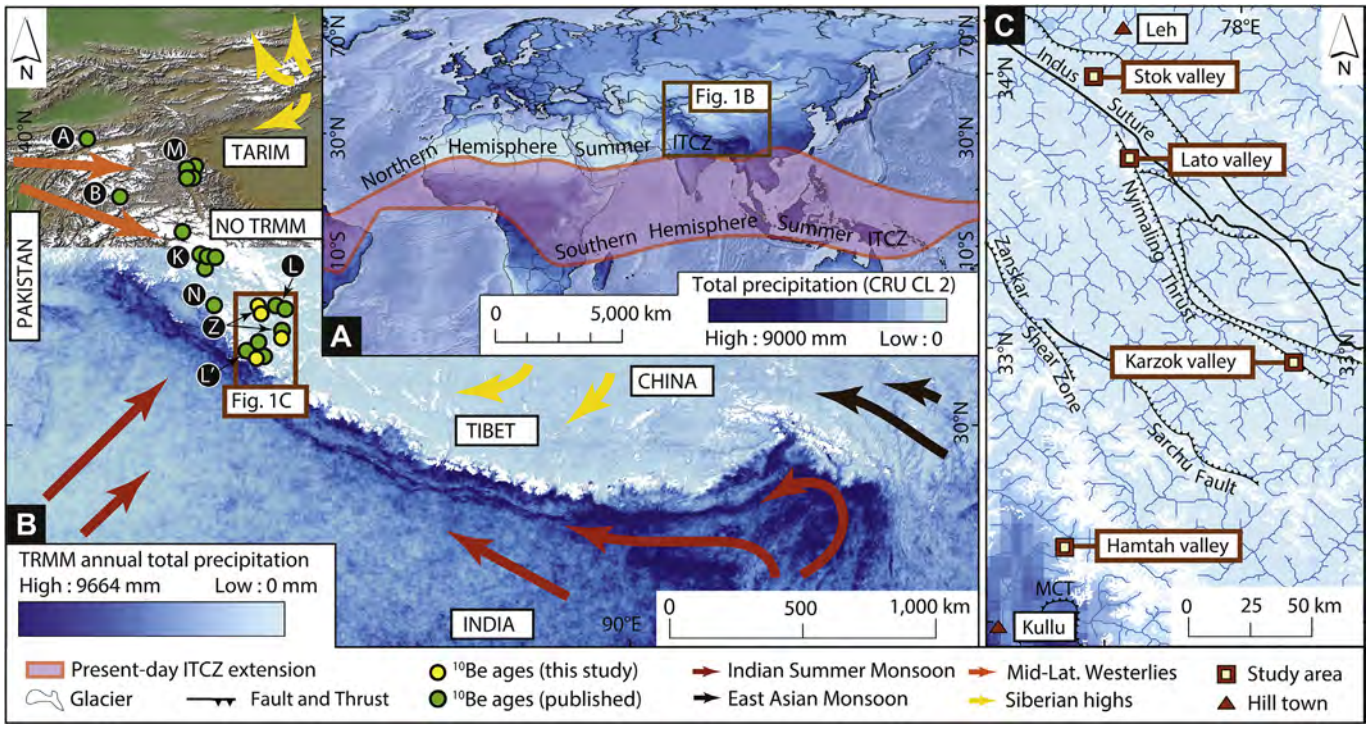

Fig. 1. Regional context and location of the study areas. (A) Present-day seasonal distribution of the Intertropical Convergence Zone (ITCZ) with respect to the Himalayan-Tibetan orogen (in brown rectangle). (B) Tropical Rainfall Measuring Mission (TRMM) precipitation imagery (averaged from 1998 to 2005) superimposed on a hillshade map, showing the study area (brown rectangle) and locations of new (yellow circles) and published (green circles) ^{10}Be ages. New and published study areas are highlighted in black circles as A = Alay Range (Koksu), B = Great Bogchigir, M = Muztag Ata, K= Karakoram, L = Ladakh (Chang, Pang), N= Nun Kun, Z = Zanskar (Stok, Lato, Karzok), L' = Lahul Himal. The region is dominated by four major climate systems: the Indian summer and East Asian monsoons (during the summer), the northern mid-latitude westerlies, and the Siberian high-pressure system (during winter). (C) Locations of the new study areas showing TRMM derived strong annual total precipitation regimes from south to north. See the text for regional geology. (For interpretation of the references to color in this figure legend, the reader is referred to the Web version of this article.)

regions of the Himalayan-Tibetan orogen (Fig. 1B). These include: the Chandra valley in Lahul, (Owen et al., 2001); the Yunam (Saha et al., 2016), Puga (Hedrick et al., 2011) and Stock valleys (Orr et al., 2017) and Nun Kun massif (Lee et al., 2014) in Zanskar; the northern slopes of the Ladakh range (Dortch et al., 2013); several valleys in the eastern and central Karakoram (Owen et al., 2002; Seong et al., 2007); Muztag Ata (Seong et al., 2009) and the Great Bogchigir valley in the Pamir (Röhringer et al., 2012); and the Koksu valley in Alay Range (Abramowski et al., 2006) (Fig. 1B). These study areas are within the contemporary transition between the Indian summer monsoon and mid-latitudinal westerly climate systems. Together these represent a key natural laboratory for investigating the relative influence of these climate systems in the region (Fig. 1B).

Previous studies of Quaternary glaciation, utilizing optically stimulated luminescence (OSL) and cosmogenic ^{10}Be surface exposure ages, have shown that glacier advances at the northwestern end of the Himalayan-Tibetan orogen are likely influenced by both oscillations in the Indian summer monsoon and mid-latitude westerlies (Taylor and Mitchell, 2000; Owen et al., 2001; Hedrick et al., 2011; Dortch et al., 2013; Lee et al., 2014; Saha et al., 2016; Eugster et al., 2016; Sharma et al., 2016; Orr et al., 2017, 2018). Dortch et al. (2013) and Owen and Dortch (2014 and references therein) using ^{10}Be dating have summarized the regional Quaternary glacier advances in the northwestern end of Himalaya and Tibet. Their semi-arid western Himalayan–Tibetan stages (SWHTS) date to 311 ± 32 (SWHTS 9), ~234 ± 44 (SWHTS 7), 146 ± 18 (SWHTS 6), 121 ± 11 (SWHTS 5E), 80 ± 5 (SWHTS 5A), 72 ± 8 (SWHTS 5A), 61 ± 5 (SWHTS 4), 46 ± 4 (SWHTS 3), 30 ± 3 (SWHTS 2F), 20 ± 2 (SWHTS 2E), 16.9 ± 0.7 (SWHTS 2D), 14.9 ± 0.8 (SWHTS 2C), 13.9 ± 0.5 (SWHTS 2B), 12.2 ± 0.8 (SWHTS 2A), ~8.8 ± 0.3 (SWHTS 1E), ~6.9 ± 0.2 (SWHTS 1D), 3.8 ± 0.6 (SWHTS 1C), 1.7 ± 0.2 (SWHTS 1B), and 0.4 ± 0.1 ka (SWHTS 1A). Recently, new moraine chronologies using ^{10}Be (Saha et al., 2016, Eugster et al., 2016; Orr et al., 2017, 2018) and OSL (Sharma et al., 2016) are also added to further improve and corroborate the existing regional stages of Quaternary glacier advances. While detailed Pleistocene chronologies are reconstructed in several valleys in the northwestern Himalaya, only a few attempts have been made to reconstruct Holocene glacial chronostratigraphies in the Lahul and Zanskar regions (see Owen and Dortch, 2014). These studies have delineated how small temperate to sub-polar glaciers in these regions oscillated throughout the Holocene. We, therefore, selected areas across the northwestern end of the Himalayan-Tibetan orogen which have a strong precipitation gradient, ranging from ~800 to ~40 mm a^{-1}, to help examine Holocene glacier oscillations. From wettest to driest, our study areas include the Hamtah valley in the Lahul Himalaya, and the Karzok, Lato, and upper Stok valleys in Zanskar (Fig. 1). We use ^{10}Be dating because this method has been applied extensively due to scarcity of suitable organic materials necessary for radiocarbon dating and/or the lack of well-bleached non-glacial sediments suitable for OSL dating (Owen and Dortch, 2014). The primary goals of our study are to refine previously proposed regional glacial stages (Dortch et al., 2013; Owen and Dortch, 2014; Solomina et al., 2015) and to assess whether Holocene glacier advances at the northwestern end of the Himalayan-Tibetan orogen were driven by regionally unique forcing factors that are not directly be influenced by long-term orbital trends, and/or global changes in the oceanic-atmospheric circulation system.

2. Regional setting

Our study areas encompass several tectonic-lithologic domains (Honegger et al., 1982; Brookfield and Andrews-Speed, 1984; Searle et al., 1987; Steck et al., 1998; Schlup et al., 2003) and are defined by three major structures. From south to north these structures are: i) the Main Central Thrust (MCT); ii) the Zanskar Shear Zone (ZSZ) and the Sarchu fault; and iii) Indus-Tsangpo Suture Zone (ITSZ) (Fig. 1C; Epard and Steck, 2008). North of the MCT, the Hamtah crystalline axis consists mostly of migmatites, and the Rohtang gneiss and granite (Kumar et al., 1987). The Karzok and Lato study areas, located north of ZSZ in the Zanskar range, are composed of coarse-grained granite of the North Himalayan nappe system (Stutz and Thöni, 1987; Fuchs and Linner, 1996; Steck et al., 1998; Epard and Steck, 2008). The upper reaches of the Stok study area that is located in the northwestern part of this nappe system and consists of thick-bedded conglomerates with alternating coarse and fine-grained sandstone, siltstone, and shale known as the Stok Kangri (Kangri = glacier) molasse (Brookfield and Andrews-Speed, 1984)

The Himalayan-Tibetan orogen imposes a formidable physical barrier to the Indian summer monsoon, the East Asian monsoon, and the northern mid-latitude westerlies (Fig. 1B). The present-day total annual precipitation derived from Tropical Rainfall Measurement Mission (TRMM) data for 1998 to 2005 shows a northward decline from 1500 to 3000 mm in the high mountain ranges of the Himalaya, to slightly >100 mm over much of the interior of the Tibetan Plateau (Fig. 1B; Bookhagen and Burbank, 2006). These prevailing climate systems and precipitation gradient are responsible for tropical climates in the forelands of the eastern Himalaya to sub-tropical arid climate into the interior of the Tibetan Plateau (Spicer, 2017). According to Rupper and Roe (2008) and Rupper et al. (2009), stronger monsoons are often associated with abundant moisture supply from Indian Ocean and South China Sea (Owen and Benn, 2005) and enhanced cloud albedo. Orographically modulated increased cloud albedo often favors decrease in incoming shortwave radiation (dynamic response) and in association with evaporative/sublimation cooling foster positive mass balance. This dynamic energy balance response to increased cloud cover and latent heat transfer are one of the most crucial physical mechanisms that have been argued for significantly effecting the amplitude and timing of contemporary and past Himalayan glacier oscillations (Rupper and Roe, 2008; Rupper et al., 2009). The northern mid-latitude westerlies, in contrast, teleconnect cooling events in the North Atlantic and Mediterranean regions to the Himalayan-Tibetan orogen helping regulate the supply of winter snow and fostering colder temperature (Srivastava et al., 2017). Mölg et al. (2014) has even argued that large-scale mid-latitude westerly waves play a crucial role in modulating present-day May–June precipitation and summer air temperature over monsoonal High Asia.

A strong latitudinal-temperature gradient also exists along the south-north transect, coupled with local altitudinal changes in temperature within each mountain range (CRU CL 2.0 reanalysis surface climate data derived from New et al., 2002). The contemporary regional equilibrium-line altitudes (ELAs) broadly follow the climatic gradient, rising from ~3000 m asl in the Lesser Himalaya to ~6000 m asl to the interior of Tibetan Plateau, and declining again to <4800 m asl in the northeastern part of Tibet (Benn and Owen, 1998; Zhou et al., 2011).

Most of the present-day precipitation in the study areas occurs during the summer monsoon (60–80% of annual precipitation), but both the Indian summer monsoon and the mid-latitude westerlies influence the glacier mass balance and the types of glaciers in all the study areas (Azam et al., 2014; Mölg et al., 2014). The Hamtah study area in Lahul, located in the rain shadow of the Pir Panjal range, has an annual precipitation of ~400–800 mm (Fig. 1B). The Karzok, Lato, and Stok study areas, to the north of the Transhimalaya, have annual precipitation ranging from 40 to 100 mm (Fig. 1B and C). Temperate glaciers in the Greater Himalaya, to the south, including Lahul, are larger, more erosive, melt-dominated, and support a thick debris-mantle in the ablation zone (Benn and Owen, 2002). These glaciers presently receive abundant snowfall during the summer monsoon and are more susceptible to changes in temperature (see Su and Shi, 2002). In contrast, glaciers in the northern and northwestern parts of the study areas, that include the northern Zanskar and Ladakh ranges, Central Karakoram, the Pamir, and Alay Ranges (Fig. 1B) are predominantly of cold-based sub-polar types, they are smaller, mostly debris free, and are more precipitation-sensitive and sublimation dominated (Benn and Owen, 2002). Presently most of these glaciers are fed by the snowfall associated with the winter mid-latitude westerlies system (Fig. 1B), and directly respond to changes in the strength of westerly-winds.

3. Methods

3.1. Geomorphic mapping

Former glacier extents in each of the study areas were reconstructed by mapping glacial and associated landforms in the field using a handheld GPS at the scale of 1:20,000 (uncertainty ±3 m; Fig. 2). High resolution Google Earth imagery, Advanced Spaceborne Thermal Emission and Reflection Radiometer (ASTER) global digital elevation models (V002, resolution of 30 m), and Landsat Enhanced Thematic Mapper Plus (ETM+) imagery (resolution 30 m) were used to aid in reconnaissance and final field mapping (http://glovis.usgs.gov/next/). Contemporary and past glacier maps of all previously investigated (dated using ^{10}Be) glaciated valleys (Fig. 1B; Supplementary material S1) were also prepared using the satellite imagery and published geomorphic maps.

3.2. Morphostratigraphy

Moraines and associated landforms in the four study areas were assigned to glacial stages based on morphostratigraphy using the scheme proposed by Hughes et al. (2005) and Hughes (2010). We used the letters *m* to denote moraines and *b* for glacially eroded bedrock. Subscript letters are used to indicate the study area, e.g., *H* for Hamtah study area (Fig. 2A). Individual moraines and bedrock surfaces were also numbered using a subscript (*1, 2 … n*) from youngest to oldest. Furthermore, individually mapped moraine ridges (ice-contact ridges) within a moraine set of a particular glacial stage were assigned a subscript letter *a, b … n* (with increasing age). For instance, the m_{H1a} is a moraine (*m*) in the Hamtah study area (subscript *H*), it is the youngest moraine (subscript *1*) and the youngest ridge (subscript *a*), whereas the m_{H3a} is a moraine with a single ridge (subscript *a*) and is the oldest of a set of three moraines (subscript 3).

3.3. Sampling for cosmogenic ^{10}Be

Moraine boulders and glacially sculpted bedrock surfaces were sampled based on the morphostratigraphic considerations; only sharp-crested, relatively well-preserved moraines with little evidence of erosion and/or degradation were sampled (Table 1; Fig. 3; Supplementary material S2). Multiple (9–3) boulder samples were

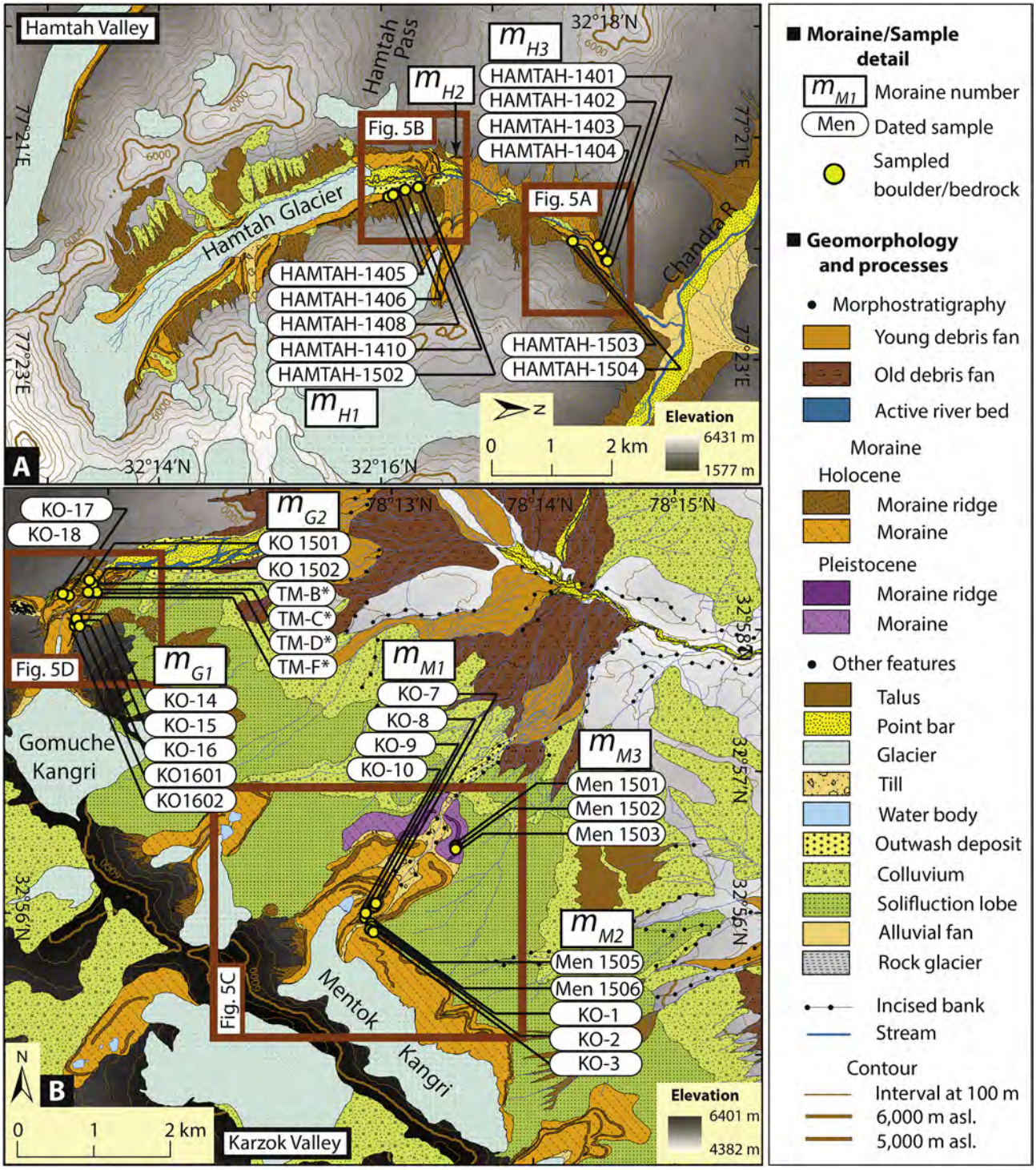

Fig. 2. Geomorphology of the study areas. (A) Hamtah valley showing locations of moraine boulders. (B) Karzok valley highlighting the sample locations. Four published samples (*) on older m_{G2} moraine are adapted from Hedrick et al. (2011). (C) Landforms and locations of sampled moraine boulders in the Lato valley. (D) Stok valley showing sampling locations for m_{S1} moraine complex. Published samples (*) for m_{S1} are adapted from Orr et al. (2017). Note: the maps are based on UTM projection (Zone 43N) and WGS 1984 datum.

obtained from individual moraines. We only sampled quartz-rich large boulders (>50 cm high) that were inset into the crest of moraines and showed no evidence of post-depositional toppling and little, if any, weathering (Table 2; Fig. 3). We generally avoided sampling boulders close to hillslopes, on moraine slopes, or within depressions that might be affected by post-depositional toppling, exhumation, and shielding. Intensely jointed, fractured, pitted, and/or sediment covered boulders were avoided to reduce the possibility that the boulders might have had complex exposure histories. Boulders with well-developed rock varnish and/or lichen cover were preferentially sampled; these features provide a measure of confidence that the boulders had not recently toppled and/or have

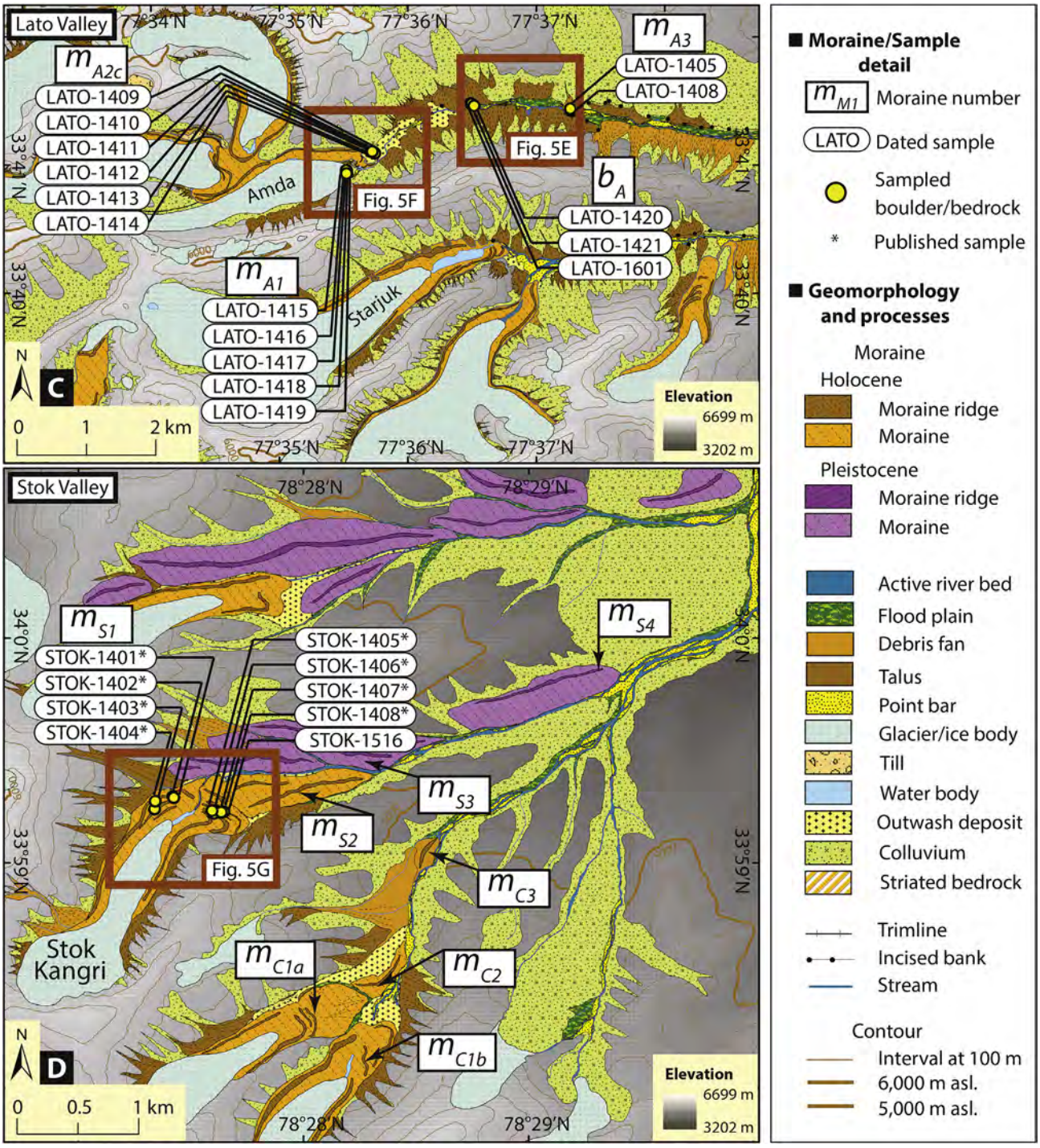

Fig. 2. (*continued*).

been recently exhumed.

Approximately 500 g of rock from the top (to a depth of ≤3) of each boulder/bedrock surface were collected using a hammer and chisel (Table 2). Topographic shielding was recorded using a clinometer and compass, measuring the skyline angles above the horizontal to the skyline at azimuth intervals of 10° (Gosse and Phillips, 2001; Balco et al., 2008). Boulders were photographed from several perspectives and their locations were recorded using a handheld GPS (Fig. 3; Supplementary material S2). The width, length and height of each boulder were documented using a tape measure (Table 2).

3.4. ^{10}Be extraction and AMS measurements

Quartz extraction and ^{10}Be sample preparation were performed in the Geochronology Laboratories at the University of Cincinnati using the community standard methods of Nishiizumi et al. (1994) and Kohl and Nishiizumi (1992). All AMS measurements were performed at the Purdue Rare Isotope Measurement (PRIME) Laboratory at Purdue University (Sharma et al., 2000). Be isotopic

Table 1
Descriptions of morphostratigraphically defined glacial landforms in our study areas.

Glacial Stage	Moraine/bedrock characteristics	Boulder characteristics
Hamtah valley, Lahul		
m_{H1a}	— Innermost latero-frontal moraine with sharp crest; pebbly/boulder diamicton with sandy-gravel matrix; prominent ablation valley separates the morainic boulder from the debris fans/talus; several hummocky ridges are present in the frontal section of the moraine; grasses are present.	— Angular to subangular large boulders along the crests of the moraine; tabular and moderately to well inset; slightly dip down the ablation valley supporting its glacial origin; no sign of slope deposition; very coarse grained leucogranite; several lichen-covered large boulders are present.
m_{H1b}	— ~2-km-long sharp-crested latero-frontal moraine; ~20 m relief from the valley floor; next to one of the hanging glaciers to the east; situated ~200 m above the present main valley floor at an altitude of 4150 −4540 m asl.	— Not dated; mostly angular to subangular boulders.
m_{H2}	— A lateral moraine remnant ~200 m down valley from *mH1a* and is at an altitude of 3980−3990 m asl. The western lateral moraine is mostly buried under debris flow fans and scree, although there is a <100-m-long stretch that is only partially buried.	— Not dated; no suitable boulders are available.
m_{H3}	— ~2.4-km-long outermost lateral moraine; presently the frontal section of the moraine is being eroded/incised; extensively covered by grasses and soil development; pebbly diamicton with sandy-gravel matrix; prominent ablation valley is present to the west.	— Subangular/subrounded leucogranite boulders distributed along the crests of the two moraine ridges; mostly stable, tabular and well inset; largely covered by lichens.
Mentok Kangri, Karzok		
m_{M1}	— ~2.5-km-long, well-preserved, steep, sharp-crested latero-frontal moraine with four recessional ice-contact ridges; samples are collected from all four ridges; pebbly diamicton with sandy-gravel matrix.	— Angular to subangular fresh, large, tabular granitic and metagranitic boulders; little to no weathering and/or toppling; inset on the crest of the moraine, especially well interlocked with other boulders.
m_{M2}	— ~7-km-long discontinuous latero-frontal moraine; consists of four ice-contact ridges; pebbly till deposit with sandy-gravel matrix; a few very small localized patches of xerophytic shrubs and grasses.	— Little to slightly weathered and fresh granitic and metagranitic rocks; large tabular boulders on the crest of the moraine; stable fresh fracture faces (angular/subangular) and distinct from older fracture faces; mostly well interlocked with other boulders.
m_{M3}	— Single lateral ridge with a rounded crest; rock varnish present in most boulders; patches of xerophytic shrubs, grasses, mosses and lichens are present; sandy-gravelly matrix.	— Well inset large granitic boulders into the moraine crest; moderate to high granular weathering with rounded top; the protruding top portion were sampled; hard to sample.
Gomuche Kangri, Karzok		
Contemporary (unstable)	— Very unstable micro-ridge close to present glacier snout; buried ice is exposed at many places; probably-boulder surface till is constantly degrading, likely turn into ground till in future; sandy matrix is present in exposed sections; geometry of the moraine ridges and presence of boulder tables indicate that this section was once part of the main glacier body.	— Not dated; boulders are not stable and suitable for exposure dating.
m_{G1}	— ~2.2-km-long latero-frontal moraine; pebbly till deposit with sandy-gravelly matrix; three prominent ridges were mapped; average height of the ridges is 23 m above the valley floor; mosses and lichens are present in patches but less.	— Fresh angular and subangular metagranitic boulders mostly well interlocked with other boulders and stable at the crest; little to not weathered.
m_{G2} (or KM-4)	— The moraine ridge complex is discontinuous and highly degraded with multiple tens of meters long recessional and hummocky ridges; likely part of a dead-ice zone; samples collected on the farthest downstream recessional ridges; fresh boulder surface with pebbly diamicton and supported by sand-gravelly matrix.	— large (~2-m-tall), tabular, and well-inset porphyritic granitic boulders from the most stable ridge crests; subangular/angular large blocks; patches of mosses and lichens are present but not extensive; some to no weathering was identified; hard to sample.
Amda valley, Lato		
m_{A1}	— ~154-m-long and 20-m-high end moraine; exhibits little, if any, signs of erosion/degradation; diamicton of boulders and cobbles present with clasts supported by coarse gravel-sandy matrix; stable ridge.	— Freshly fractured and tabular granitic boulders; no sign of weathering; very limited to no detrital materials on the boulders surface; lodged on the crest of the end moraine.
m_{A2a}	— A ~120-m-long subdued (~8 m relief) recessional moraine, located ~75 m downstream of *mA1;* slightly unstable and presently is being incised by anastomosing outwash streams.	— Not dated; lack of suitable boulders.
m_{A2b}	— ~110-m-long and ~6-m-high subdued dissected ridge; slightly unstable.	— Not dated; lack of suitable boulders.
m_{A2c}	— ~346-m-long and 10-m-high end moraine; diamicton of boulders and cobbles present with clasts supported by coarse gravel-sandy matrix; stable ridge with rounded surface; some very small patches of some xerophytic shrubs and grasses are present.	— Fresh angular and subangular porphyritic granite boulders; boulder inset on the crests away from the depression; boulders are mostly well interlocked with other boulders.
b_a	— Glacially sculpted striated bedrock; highly polished and striated flat surface; striations are parallel to ice flow.	— Samples were collected from smooth polished surfaces at different elevations; extensive lichen cover and rock varnish present.
m_{A3}	— 10-m-high end moraine; northern part of the moraine is subdued; striated boulders are lodged on the surface with diamicton of boulders and cobbles; south facing slope likely covered by post-depositional slope deposits; some xerophytic shrubs and grasses present.	— Larger tabular granitic boulders; subangular/subrounded; some boulders are slightly lichen covered; some boulders are slightly denuded.
Stok valley, Zanskar		
m_{S1}	— ~30-m-high and 2.8-km-long latero-frontal moraine complex; consisting of >4 ice-contact inner recessional ridges; outer ridge is narrow, steep and more prominent; inner frontal ridges are subdued; diamicton of highly fractured boulders and cobbles with coarse gravel-sandy matrix; slight lichen cover.	— Angular to subangular boulders; large vein-quartz dominated conglomerate boulders; fresh fractures and sharp edges indicate slightly to moderately denudated; partially inset but appeared stable; boulder fracturing due to thermal shock and post-depositional block displacement is evident.
m_{S2}	— Consisting of two rounded/denudated ice-contact ridges and is located ~400 m downstream of m_{S1}; coarse gravel-sandy matrix supported.	— Not dated; highly denudated rounded boulders; mostly large and stable but highly pitted and fractured granites; rock varnish and extensive lichen cover exists.

Table 1 (*continued*)

Glacial Stage	Moraine/bedrock characteristics	Boulder characteristics
Stok companion glacier, Zanskar		
m_{C1a}	— Slightly unstable; freshly exposed laterofrontal moraine ridge; pebbly-boulder diamicton with sandy-gravel matrix.	— Not dated; angular to subangular fresh tabular boulders; well inset on the crest; highly fractured due to its lithology.
m_{C1b}	— Slightly unstable young laterofrontal moraine ridge; pebbly-boulder diamicton with sandy-gravel matrix.	— Not dated; angular to subangular fresh tabular boulders; highly fractured due to its lithology.
m_{C2}	— Stable lateral moraine ridge; pebbly-boulder diamicton with sandy-gravel matrix.	— Not dated; angular to subangular fresh tabular boulders.
m_{C3}	— Round crested lateral moraine remnant; well stable, but denudated surface; some xerophytic shrubs and grasses present.	— Not dated; highly denudated conglomerate boulders; mostly large and stable but highly pitted and fractured granites; rock varnish and extensive lichen cover exists.

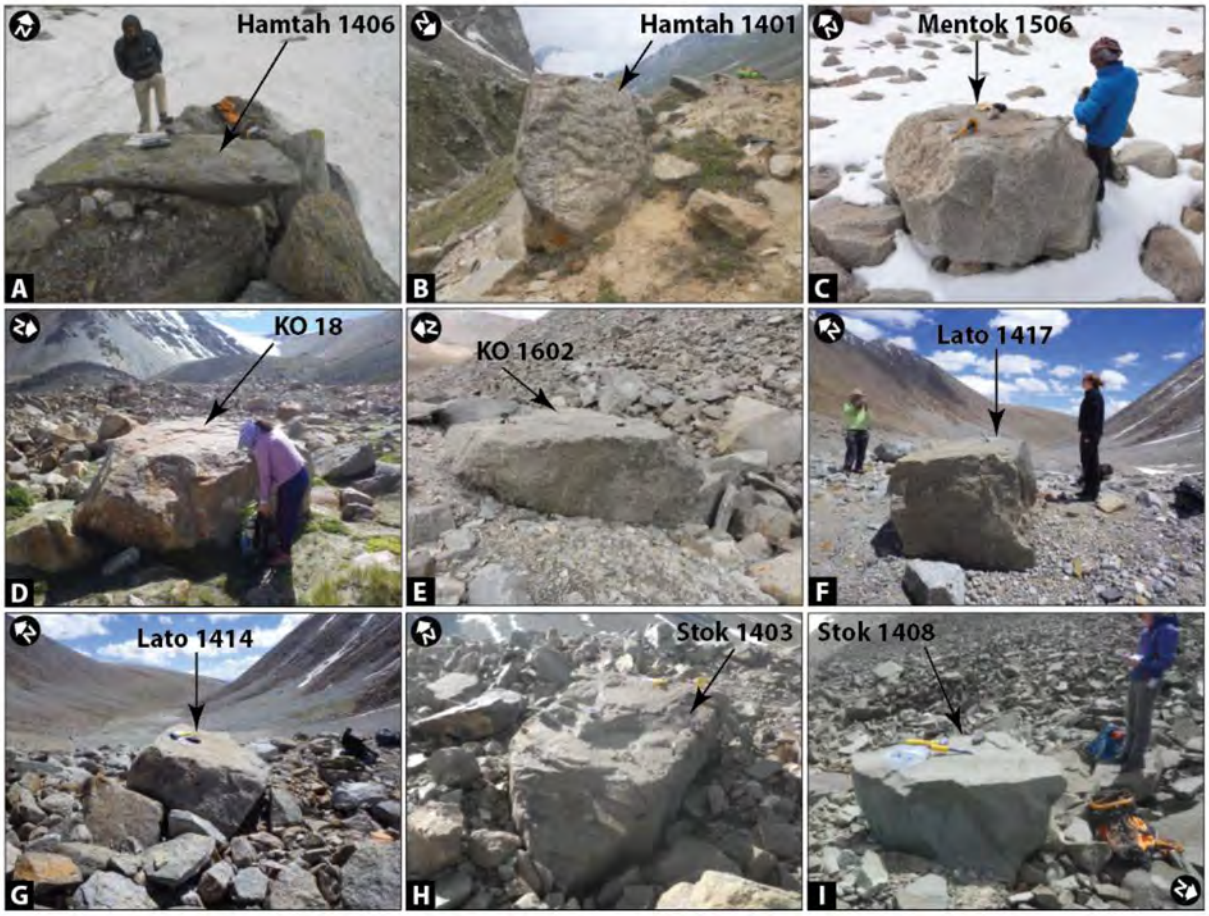

Fig. 3. Examples of sampled boulders for ^{10}Be exposure dating. Boulders inset into m_{H1a} latero-frontal (A) and m_{H3} lateral (B) moraines of the Hamtah study area. (C) A large tabular boulder resting on m_{M1} latero-frontal moraine of Mentok Kangri. (D and E) Boulders resting on the outer m_{G2} and the innermost m_{G1} latero-frontal moraines of Gomuche Kangri, respectively. (F and G) Boulders standing upright at the crest of m_{A1} and m_{A2c} end moraines in Lato study area, respectively. (H and I) Views of boulders embedded into the crest of young m_{S1} moraine complex of Stok study area.

measurements were normalized using the 07KNSTD standard (Nishiizumi et al., 2007). We used the appropriate standard correction factors available at http://hess.ess.washington.edu/for recalculating published ages. Residual boron contamination was considered negligible and no correction for boron was made in the age calculation (cf. Putnam et al., 2013b; Corbett et al., 2016). Blank corrections ranged from 0.1 to 23.1% (averaging 3%) for a ^{10}Be concentration of >20,000 atoms g^{-1} SiO_2 and from 15.7 to 32.4% for a ^{10}Be concentration of <20,000 atoms g^{-1} SiO_2. Analytical uncertainties were generally 5.8 ± 5.1% (±1σ), but larger than 10% for five very young samples (<0.6 ka; Table 2).

3.5. Exposure age calculations

Exposure ages were determined using the CRONUScale (Marrero et al., 2016), Cosmic Ray Exposure program (CREp; Martin et al., 2016) and CRONUS-Earth V3 (http://hess.ess.washington.edu/math/v3/v3_age_in.html) online calculators (Supplementary material S3). There are several notable differences among these recent age calculators, most prominent being the sea-level high-latitude (SLHL) spallogenic production rates. In the absence of a locally calibrated *in situ* ^{10}Be production rate (Heyman, 2014), we used the global SLHL production rates of ~3.92 ± 0.17 atoms g^{-1} a^{-1} in the CRONUScale (Borchers et al., 2016; Marrero et al., 2016) and

Table 2
Holocene moraine/bedrock surface-exposure sample details and ^{10}Be ages (in thousands of years before 2016 CE, labeled 'ka'±1σ) for the four study areas of the northwestern Himalaya.

Area	Moraine morpho-stratigraphy	Sample ID	Latitude (° N)	Longitude (° E)	Elevation (m asl)	Boulder size (LxWxH) (cm)	Sample thickness (cm)	Shielding correction	Quartz weight (g)	Carrier added (g)	^{10}Be/^{9}Be ± 1σ (10^{-15})[g]	[^{10}Be] ± 1σ (10^{4} atoms g^{-1})[h]	LSD Age ± 1σ (ka)[i]	Lm Age ± 1σ (ka)[i]
Hamtah valley	m_{H1a}	HAMTAH-1405	32.2725	77.3574	4014	410 × 390 x 120	2.0	0.943	28.9662	0.3515[d]	10.74 ± 2.32	0.89 ± 0.19	0.23 ± 0.05	0.21 ± 0.05
	m_{H1a}	HAMTAH-1406	32.2722	77.3575	4023	190 × 80 x 60	1.0	0.944	29.5368	0.3510[d]	19.17 ± 5.08	1.56 ± 0.41	0.40 ± 0.11	0.37 ± 0.10
	m_{H1a}	HAMTAH-1408[a]	32.2686	77.3585	4111	160 × 100 x 60	2.5	0.954	25.6686	0.3515[e]	96.62 ± 5.90	9.06 ± 0.55	2.35 ± 0.22	2.21 ± 0.18
	m_{H1a}	HAMTAH-1410	32.2678	77.3589	4125	130 × 80 x 70	2.5	0.948	25.3997	0.3503[d]	6.30 ± 1.08	0.60 ± 0.10	0.14 ± 0.03	0.13 ± 0.03
	m_{H1a}	HAMTAH-1502[a]	32.2954	77.3655	3861	300 × 210 x 200	2.0	0.923	22.1344	0.3518[f]	24.13 ± 2.31	2.57 ± 0.25	0.74 ± 0.09	0.70 ± 0.07
	m_{H3}	HAMTAH-1401	32.3005	77.3684	3783	110 × 100 x 110	1.5	0.897	25.6264	0.3501[d]	398.76 ± 20.43	37.33 ± 1.91	10.94 ± 0.66	10.48 ± 0.62
	m_{H3}	HAMTAH-1402[a]	32.3006	77.3685	3769	160 × 120 x 60	2.0	0.887	26.2449	0.3503[d]	217.14 ± 18.51	19.86 ± 1.69	6.24 ± 0.51	5.93 ± 0.48
	m_{H3}	HAMTAH-1403[a]	32.2998	77.3670	3808	250 × 150 x 80	1.0	0.879	27.8189	0.3513[d]	670.80 ± 27.12	58.05 ± 2.35	16.18 ± 1.03	15.67 ± 0.87
	m_{H3}	HAMTAH-1404[a]	32.2992	77.3662	3808	360 × 270 x 100	2.0	0.879	25.2556	0.3523[e]	128.03 ± 6.02	12.21 ± 0.57	4.05 ± 0.28	3.79 ± 0.23
	m_{H3}	HAMTAH-1503	32.2685	77.3586	4112	270 × 180 x 100	3.0	0.898	7.7449	0.3506[e]	131.06 ± 2.72	41.47 ± 0.86	10.36 ± 0.53	10.02 ± 0.47
	m_{H3}	HAMTAH-1504	32.2703	77.3579	4083	570 × 270 x 220	3.0	0.879	23.2097	0.3497[f]	384.84 ± 7.21	38.89 ± 0.73	10.13 ± 0.54	9.77 ± 0.47
Lato valley	m_{A1}	LATO-1415[a]	33.6822	77.5920	5366	200 × 130 x 90	3.0	0.95	22.2096	0.3518[f]	125.27 ± 2.91	13.31 ± 0.31	1.78 ± 0.11	1.72 ± 0.11
	m_{A1}	LATO-1416	33.6822	77.5921	5358	590 × 290 x 110	4.0	0.95	25.2732	0.3498[d]	17.46 ± 1.86	1.66 ± 0.18	0.21 ± 0.03	0.20 ± 0.03
	m_{A1}	LATO-1417	33.6826	77.5920	5348	185 × 140 x 100	2.0	0.951	28.3242	0.3506[d]	32.31 ± 1.17	2.74 ± 0.10	0.35 ± 0.03	0.34 ± 0.03
	m_{A1}	LATO-1418	33.6826	77.5921	5351	70 × 40 x 70	3.0	0.946	24.7312	0.3505[d]	18.41 ± 1.47	1.79 ± 0.14	0.22 ± 0.03	0.22 ± 0.03
	m_{A1}	LATO-1419[a]	33.6827	77.5920	5339	110 × 80 x 40	3.0	0.952	23.038	0.3523[f]	240.38 ± 18.05	24.66 ± 1.85	3.43 ± 0.32	3.31 ± 0.32
	m_{A2c}	LATO-1409[a]	33.6851	77.5953	5314	180 × 150 x 60	3.0	0.959	11.5494	0.3505[d]	1274.75 ± 27.10	265.10 ± 5.64	27.56 ± 1.52	29.25 ± 1.52
	m_{A2c}	LATO-1410[a]	33.6851	77.5953	5321	180 × 110 x 50	2.5	0.959	28.05	0.3511[d]	254.86 ± 10.13	21.86 ± 0.87	3.04 ± 0.21	2.93 ± 0.21
	m_{A2c}	LATO-1411[a]	33.6851	77.5952	5315	250 × 160 x 90	2.0	0.959	27.7016	0.3512[d]	341.11 ± 20.48	29.63 ± 1.78	4.06 ± 0.32	3.92 ± 0.32
	m_{A2c}	LATO-1412	33.6850	77.5957	5315	210 × 80 x 70	1.0	0.958	24.1378	0.3514[e]	27.71 ± 1.47	2.76 ± 0.15	0.35 ± 0.03	0.34 ± 0.03
	m_{A2c}	LATO-1413	33.6849	77.5957	5317	170 × 80 x 60	2.0	0.959	23.0324	0.3501[f]	56.57 ± 2.00	5.77 ± 0.20	0.74 ± 0.06	0.73 ± 0.06
	m_{A2c}	LATO-1414	33.6851	77.5954	5314	200 × 130 x 100	2.0	0.96	27.964	0.3509[d]	43.71 ± 2.12	3.76 ± 0.18	0.48 ± 0.03	0.46 ± 0.03
	b_A	LATO1420[b]	33.6914	77.6081	5191	Bedrock	2.5	0.951	11.888	0.3516[e]	544.04 ± 14.91	110.02 ± 3.02	13.73 ± 0.74	13.9 ± 0.74
	b_A	LATO1421[b]	33.6913	77.6083	5180	Bedrock	3.0	0.951	17.4754	0.3489[e]	790.62 ± 16.30	107.92 ± 2.22	13.61 ± 0.7	13.77 ± 0.7
	b_A	LATO1601[b]	33.6911	77.6086	5171	Bedrock	2.0	0.942	12.0054	0.3521[e]	560.06 ± 8.24	114.80 ± 1.69	14.43 ± 0.7	14.65 ± 0.7
	m_{A3}	LATO1405[a]	33.6805	77.6211	5134	150 × 130 x 50	2.0	0.968	27.9485	0.3502[e]	172.80 ± 114.18	14.80 ± 9.78	2.15 ± 1.42	2.08 ± 1.42
	m_{A3}	LATO1408[a]	33.6907	77.6211	5136	120 × 90 x 50	1.0	0.971	28.7324	0.3502[e]	137.57 ± 20.37	11.46 ± 1.70	1.62 ± 0.27	1.57 ± 0.27
Stok valley	m_{S1}	STOK-1405[c]	33.9872	77.4601	5370	140 × 70 x 70	2.0	0.98	25.0795	0.3522[e]	79.59 ± 3.26	7.64 ± 0.31	0.93 ± 0.07	0.92 ± 0.07
	m_{S1}	STOK-1406[a c]	33.9870	77.4600	5314	160 × 80 x 100	2.5	0.98	25.6799	0.3507[d]	48.48 ± 2.35	4.54 ± 0.22	0.56 ± 0.04	0.55 ± 0.04
	m_{S1}	STOK-1407[a c]	33.9871	77.4608	5340	290 × 200 x 190	3.0	0.978	26.4547	0.3514[d]	13.71 ± 2.35	1.25 ± 0.21	0.14 ± 0.03	0.14 ± 0.03
	m_{S1}	STOK-1408[c]	33.9871	77.4606	5308	190 × 130 x 100	3.0	0.978	10.6812	0.3483[d]	41.68 ± 3.21	9.31 ± 0.72	1.19 ± 0.11	1.17 ± 0.11
	m_{S1}	STOK-1516	33.9872	77.4599	5303	160 × 120 x 70	3.0	0.977	22.944	0.3519[f]	71.67 ± 6.36	7.37 ± 0.65	0.94 ± 0.1	0.92 ± 0.1
	m_{S1}	STOK-1401[c]	33.9873	77.4557	5329	120 × 90 x 100	3.0	0.964	25.5582	0.3505[e]	165.80 ± 5.43	15.57 ± 0.51	2.06 ± 0.14	2.00 ± 0.14

	m_{S1}	STOK-1402[c]	33.9879	77.4557	5330	180 × 160 x 100	3.0	0.967	25.2641	0.3498[e]	123.78 ± 6.10	11.72 ± 0.58	1.51 ± 0.12	1.48 ± 0.12
	m_{S1}	STOK-1403[c]	33.9883	77.4570	5323	140 × 70 x 70	1.0	0.969	26.8263	0.3503[e]	164.10 ± 7.28	14.65 ± 0.65	1.89 ± 0.14	1.84 ± 0.14
	m_{S1}	STOK-1404[a c]	33.9882	77.4571	5328	280 × 130 x 80	2.0	0.969	25.2253	0.3509[d]	21.87 ± 0.90	2.08± 0.09	0.25 ± 0.02	0.25 ± 0.02
Karzok valley	m_{M1}	KO-7[a]	32.9328	78.2136	5524	250 × 160 x 100	6.0	1.000	25.6596	0.3513[e]	21.74 ± 1.45	2.04 ± 0.14	0.24 ± 0.02	0.23 ± 0.02
	m_{M1}	KO-8	32.9333	78.2136	5516	170 × 130 x 90	2.5	1.000	25.4739	0.3497[e]	63.04 ± 5.85	5.92 ± 0.55	0.69 ± 0.08	0.68 ± 0.08
	m_{M1}	KO-9	32.9341	78.2147	5503	380 × 240 x 260	1.0	1.000	25.2789	0.3497[e]	63.36 ± 2.49	6.00 ± 0.24	0.70 ± 0.05	0.68 ± 0.05
	m_{M1}	KO10	32.9345	78.2148	5503	160 × 130 x 90	1.0	1.000	22.2821	0.3489[e]	44.16 ± 6.22	4.73 ± 0.67	0.54 ± 0.09	0.53 ± 0.09
	m_{M2}	KO1[a]	32.9321	78.2143	5532	300 × 160 x 80	3.0	1.000	22.4344	0.3504[e]	191.11 ± 6.14	20.44 ± 0.66	2.56 ± 0.19	2.46 ± 0.19
	m_{M2}	KO-2	32.9317	78.2143	5541	400 × 325 x 140	6.0	1.000	21.9943	0.3507[d]	82.65 ± 4.89	9.03 ± 0.53	1.09 ± 0.09	1.07 ± 0.09
	m_{M2}	KO-3	32.9314	78.2142	5548	140 × 60 x 100	4.0	0.991	25.8534	0.3530[e]	87.60 ± 4.20	8.18 ± 0.39	0.98 ± 0.07	0.95 ± 0.07
	m_{M2}	MENTOK-1505	32.9312	78.2145	5569	190 × 130 x 90	2.0	0.991	22.3311	0.3503[f]	83.27 ± 3.05	8.76 ± 0.32	1.02 ± 0.07	1.00 ± 0.07
	m_{M2}	MENTOK-1506	32.9311	78.2145	5574	190 × 160 x 110	1.0	0.992	22.115	0.3517[f]	73.53 ± 4.69	7.84 ± 0.50	0.90 ± 0.08	0.88 ± 0.08
	m_{M3}	MENTOK-1501	32.9413	78.2242	5331	200 × 170 x 90	2.0	1.000	24.3921	0.3530[f]	5669.39 ± 54.77	550.34 ± 5.32	57.21 ±3.51	60.02 ± 3.51
	m_{M3}	MENTOK-1502[a]	32.9411	78.2242	5335	340 × 170 x 100	2.0	1.000	24.2451	0.3519[f]	3694.63 ± 69.15	359.70 ± 6.73	36.49 ±1.99	38.32 ± 1.99
	m_{M3}	MENTOK-1503[a]	32.9408	78.2242	5339	410 × 300 x 320	2.0	1.000	24.5983	0.3515[f]	2302.94 ± 27.85	220.73 ± 2.67	22.86 ±1.08	23.76 ± 1.08
	m_{G1}	KO-14	32.9672	78.1794	5374	200 × 190 x 150	3.0	0.961	19.5522	0.3513[d]	138.87 ± 5.85	17.10 ± 0.72	2.36 ± 0.19	2.27 ± 0.19
	m_{G1}	KO-15[a]	32.9678	78.1796	5366	270 × 240 x 110	3.0	0.966	29.9259	0.3504[d]	61.45 ± 3.22	4.93 ± 0.26	0.64 ± 0.05	0.62 ± 0.05
	m_{G1}	KO-16[a]	32.9678	78.1796	5366	400 × 300 x 270	4.0	0.966	15.4506	0.3513[d]	24.82 ± 2.04	3.87 ± 0.32	0.5 ± 0.06	0.48 ± 0.06
	m_{G1}	KO1601	32.9680	78.1796	5374	270 × 210 x 100	2.0	0.966	25.5064	0.3503[e]	139.61 ± 4.08	13.40 ± 0.39	1.79 ± 0.12	1.73 ± 0.12
	m_{G1}	KO1602	32.9671	78.1800	5388	200 × 120 x 140	1.5	0.954	9.4984	0.3524[e]	73.03 ± 2.75	18.94 ± 0.71	2.61 ± 0.19	2.51 ± 0.19
	m_{G2}	KO-17	32.9706	78.1787	5331	307 × 109 x 190	3.0	0.984	16.6632	0.3505[d]	163.54 ± 6.74	23.57 ± 0.97	3.29 ± 0.23	3.16 ± 0.23
	m_{G2}	KO-18	32.9708	78.1780	5337	290 × 190 x 180	2.0	0.985	27.5274	0.3519[d]	419.49 ± 13.55	36.75 ± 1.19	4.93 ± 0.28	4.74 ± 0.28
	m_{G2}	KO-1501	32.9720	78.1815	5327	370 × 290 x 150	1.0	0.99	22.2012	0.3514[f]	451.84 ± 11.51	47.97 ± 1.22	6.05 ± 0.3	5.92 ± 0.3
	m_{G2}	KO-1502[a]	32.9724	78.1812	5334	300 × 260 x 220	2.0	0.99	24.2361	0.3510[f]	1090.46 ± 13.90	105.93 ± 1.35	12.37 ±0.7	12.42 ± 0.7

Note: Density value of 2.7 g cm^{-3}, erosion rate of 0.00 cm a^{-1}, and AMS standard of 07KNSTD were used for all samples to calculate surface exposure ages. For lithology, please see the Section 2 and Table 1.
Lato ^{10}Be ages are also reported in Orr et al., 2018 which was submitted parallel with this manuscript.

[a] Outliers are identified and removed. Detail statistics are discussed in Table S1.
[b] Bedrock samples.
[c] Published ^{10}Be ages from Orr et al., 2017.
[d] Carrier ^{9}Be concentration is 1025.5 ppm.
[e] Carrier ^{9}Be concentration is 1023.2 ppm.
[f] Carrier ^{9}Be concentration is 1003.8 ppm.
[g] Ratios are corrected from background ^{10}Be detected in procedural blanks
[h] Reported (^{10}Be) values have been corrected om background ^{10}Be detected in procedural blanks
[i] Lifton-Sato-Dunai (LSD) scaling model using CREp online calculator.
[j] Lal and Stone time-dependent (Lm) scaling model using CREp online calculator.

4.08 ± 0.23 atoms g^{-1} a^{-1} in the CREp and CRONUS-Earth V3 calculators that are linked to the online ICE-D database (Martin et al., 2016). All available scaling models, i.e., Lifton-Sato-Dunai (LSD; Lifton et al., 2014 [SA and SF in Marrero et al., 2016]), Lal and Stone time-dependent (Lm; Balco et al., 2008), Lal and Stone time-independent (St; Lal, 1991; Stone, 2000), Desilets (De; Desilets et al., 2006), Dunai (Du; Dunai, 2001), Lifton (Li; Lifton et al., 2005, 2008) were used to calculate ^{10}Be ages (Supplementary material S3). Holocene ^{10}Be age differences among different scaling frameworks computed using different age calculators were <10% (Supplementary material S4). For our study, we used the CREp LSD model when discussing the ages because the model does not have systematic neutron monitor-based biases and incorporates both time varying dipolar and non-dipolar geomagnetic components (cf., Lifton et al., 2008) and solar modulation framework (cf., Lifton et al., 2005, 2008). The CREp (LSD and Lm) ages were calculated using ERA40 atmospheric model (Uppala et al., 2005) and Lifton-VDM2016 geomagnetic database (Lifton, 2016). All the ages are reported in thousands of years (ka) before 2016 CE (the year that the new samples were processed and measured).

We assume a zero-erosion rate when calculating the ages because most of the sampled boulders exhibited little, if any, signs of weathering (e = 0 in Table 2). However, to understand how erosion might affect our Holocene ages, we experimented with several different erosion rates (Supplementary material S5). Our results suggest that even with a high steady-state erosion rate for arid and semi-arid environments, similar to our study areas, of 10 m Ma^{-1} (see Seong et al., 2007; Dietsch et al., 2015), the difference from zero erosion is <10% over the Holocene (see Supplementary material S5). No correction was made for snow cover. We argue that this is valid because most of the sampled boulders have prominent relief (rising >50 cm above the moraine surface) and likely remained snow free due to windswept conditions throughout the winter (Fig. 3). We also recalculated, using the same methods as for all new ages, the previously published ^{10}Be ages for Holocene moraines at the northwestern end of the Himalayan-Tibetan orogen (Fig. 1B; Supplementary material S6).

3.6. Moraine/bedrock ages

Geologic uncertainties including differential erosion, prior-exposure, reworking, and/or incomplete exposure histories due to exhumation of moraine boulders, that influence exposure ages often outweigh analytical and production rate uncertainties (Putkonen and Swanson, 2003; Applegate et al., 2010, 2012). These geologic uncertainties affect a mean ^{10}Be exposure age of a single landform based on multiple (9–3) samples (Table 2). Reduced chi-squared (χ^2) statistics were used to assess the distribution of ages (Applegate et al., 2010, 2012; Kaplan et al., 2013; Putnam et al., 2013b). The χ^2 values if > 1, indicates high dispersion of ages and geologic factors other than analytical uncertainties are likely accounted for. Moraine ages with $\chi^2 > 1$ are then further treated to identify outliers. Outliers were initially identified if an individual boulder age uncertainty was >2σ from the arithmetic mean age of the distribution (Putnam et al., 2013a). We further verified any outliers using Chauvenet's criterion as advocated in Taylor (1997), Dunai (2010), and Putnam et al. (2013b). Any outliers identified by these methods were additionally verified using our field records and applied only when compelling field evidence supported our statistical outliers. We were not able to apply the field verification methods for published data and hence, relied entirely on our statistical interpretation and description in respective literature (Supplementary material S3). Chosen outliers (66 out of a total of 236 ^{10}Be ages) were discarded from further statistical treatment. Finally, we report the weighted mean and 1σ uncertainties to define the true age of the moraine (Barrows, 2007). The weighted mean is usually applied in scenarios where samples are dispersed, and arithmetic mean age is likely influenced by longer tail skewed distribution (cf. Applegate et al., 2012). We have used the word 'tentative' throughout our paper as a cautionary note given possible large uncertainty associated with some of the age interpretations, especially when defining a mean based on <3 samples and/or ages for largely dispersed data.

We assume that the mean moraine ^{10}Be age is a minimum age of a local glacial stage/glacier advance as it represents the last time that boulders were deposited on the moraine before the glacier began to thin and/or retreat (cf. Gosse, 2005; Ivy-Ochs et al., 2007; Putkonen et al., 2008). We interpret bedrock ages to represent the time that a glacier withdrew from a specific location during retreat (cf. Ward et al., 2009, 2015). Moraine preservation is poor in high-energy glaciated environments such as the Himalaya due to post-depositional denudation and/or obliteration of older landscape features by advancing younger glaciers (Kirkbride and Winkler, 2012). Likewise, local microclimate, topography, hypsometry, and aspect make glaciers in some valleys more likely to respond to climate change and/or have a better-preserved record of glaciation (Roe, 2011; Barr and Lovell, 2014). Probabilistic models applied in several studies (e.g., Gibbons et al., 1984; Kirkbride and Brazier, 1998; Kirkbride and Winkler, 2012) also suggest that it is unlikely to preserve more than three sets of moraines in a single/local glaciated valley (~30% probability). We used the term *local glacial stage* to define a morphostratigraphically distinct glacier advance within any one of our four study areas. Several local glacial chronologies with similar climatic and glacial landform characteristics constitute a regional glacial stage in our study. We argue that regional glacial stages are helpful to reconstruct a complete glacial history in a region and furthermore to examine whether moraine formation has taken place due to widespread changes in climate or is due to intrinsic climate variability in individual valleys (see Roe, 2011).

3.7. Regional glacial stages

We employed radial plots (Galbraith, 1990, 2010; Galbraith and Roberts, 2012; Vermeesch, 2009) to identify different populations (local glacial stages) in preference to probability density functions (Supplementary material S3). A combination of radial plot analysis and statistical tests (student t-test) were used to test whether hypothesized age distributions were distinct from each other. A threshold two-tailed p value of <0.01 (at ≥99% confidence level) was used to define distinct regional glacial stages/chronozones. We used both the upper and lower tail distributions of the lumped age population, i.e., local glacial stages, including their uncertainties to define the chronozone of each regional glacial stage. Most regional glacial stages are based on ≥3 local glacial stages.

3.8. Equilibrium-line altitudes

We calculated former ELAs and ELA depressions (ΔELAs) for each of our study areas using detail reconstruction of former glaciers derived from our geomorphic maps, as well as all ELAs of previously ^{10}Be dated glaciated valleys using glacial maps for the northwestern end of the Himalayan-Tibetan orogen (Supplementary material S1). Assuming a simplistic steady-state scenario (Sugden and John, 1976; Putnam et al., 2013b), former ELAs were calculated using area-altitude (AA), area accumulation ratio (AAR), and toe-headwall accumulation ratios (THAR) methods for each glacier advance, as recommended by Benn et al. (2005) and Osmaston (2005; Table 3). We also used the modern maximum elevation of lateral moraines (MELM; cf. Dahl and Nesje, 1992) of

Table 3
The common AAR and THAR ratios recommended in published literature.

Study	Region	AAR	THAR
Porter (1970)	Swat Himalaya	0.6 ± 0.1	–
Andrews (1975)	Garhwal Himlaya	1.3	–
Kulkarni (1992)	Debris covered glaciers in the Western Himalaya	0.43–0.47	–
Sharma and Owen (1996)	Gangotri galcier in the Garhwal Himal	0.6 & 1.3	0.5
Burbank and Fort (1985)	Sub-polar glaciers in Ladakh region.	0.65	0.4
Fort (1995), Burbank and Cheng (1991)	Debris covered glaciers in the Nepal Himalaya	0.6–0.65	–
Taylor and Mitchell (2000)	Zanskar	–	0.4–0.5
Benn and Lehmkuhl (2000)	Debris covered glaciers in Karakoram to clean glaciers in Tibet	0.44–0.67	–
Kaser and Osmaston (2002)	Tropical debris-covered glaciers	0.65–0.70	–
Owen and Benn (2005)	Variety of glaciers in the Himalaya and Tibet	0.5–0.8	0.3–0.5
Scherler et al. (2011)	Western Himalaya	0.48 ± 26	–
Orr et al. (2017, 2018)	Zanskar	0.4, 0.5 & 0.6	0.4–0.5

studied valleys to further reconstruct modern ELAs. Calculating past ELAs based on MELM is more uncertain due to poor preservation and/or post-depositional burial of lateral moraines. Therefore, this method was not used for past glacier advances. Many of the glaciers within our study areas have widely different geometries, micro-climates, glacier hypsometries, debris mantles, and slopes, so to help address this variability we use several ELA methods. Application of multiple ELA methods also helped us to evaluate and eliminate some of the uncertainties associated with each method.

The AAR and THAR ratios used in our study were obtained from published literature for consistency and comparisons (Table 3). A selected summary of recommended AAR and THAR values are provided in Table 3. AARs vary between 0.5 and 0.7 with THARs between 0.3 and 0.5 for the majority of glacier types. When the modern AAR and THAR values (ratios) were calibrated with respect to modern MELM, the AAR and THAR had mean and 1σ values of 0.66 ± 0.13 and 0.31 ± 0.18, respectively. We calculated our ELAs based on three commonly recommended AAR (0.5, 0.6, 0.7) and THAR (0.3, 0.4, 0.5) values (Supplementary material S7). Mean ELAs and ΔELAs were calculated based on all these methods and ratio values.

4. Geomorphology of the study areas

4.1. Hamtah study area

The Hamtah study area is a north trending ~13-km-long glaciated valley that rises from 3700 m asl to the peak of Indrasan at 6223 m asl and covers an area of ~36 km^2 (Fig. 2A). The major stream, Hamtah Nala, drains from Hamtah glacier at 4070 m asl and flows into the Chandra river. The 5.7-km-long, debris-mantled Hamtah glacier, and two small glaciers occupy the valley, and have contemporary ELAs of ~4456 ± 70 m asl. While smaller hanging glaciers are located well above the present ELA and have very limited to no discernible ablation zone and the ablation zone of Hamtah glacier is large and covers ~70% (MELM derived; Shukla et al., 2015) of the total glaciated area.

Four sets of moraines are preserved in the Hamtah valley: m_{H1a}, m_{H1b}, m_{H2}, and m_{H3} (Table 1; Fig. 2A). m_{H1a} is the innermost latero-frontal moraine that has a sharp crest and extends along the valley between 3960 and 4575 m asl (Figs. 2A and 4A). The frontal section of the moraine is located at ~1 km downstream from Hamtah glacier. The western lateral moraine is discontinuous over a length of 6.3 km and covered by talus in many places (Fig. 2A). The eastern lateral moraine is a ~6-km-long, well-preserved ridge that rises ~26 m from the present valley floor. The eastern lateral moraine also preserves a distinct ablation valley parallel to its length, which helps prevent burial of the moraine by hillslope deposits. Five large boulders were sampled along this ridge (Table 1; Fig. 3A).

The outermost lateral moraine, m_{H3}, is situated ~2.4 km down valley of the m_{H1a} extending between ~3730 and 3880 m asl (Table 1; Figs. 2A and 4B). The western lateral ridge of the moraine is discontinuous over a length of ~500 m and buried by debris flows from the hillslopes. An ablation valley separates the western lateral moraine from the steep hillslope deposits in its lower reaches. Four samples were collected from this section of the moraine (Figs. 2A and 4B). The eastern lateral ridge is 660 m long with a mean height of ~10 m. While this moraine is better preserved, it is partially buried under thick rockfall deposits upstream at an altitude of >3880 m asl and downstream below <3805 m asl, where the valley narrows from ~3 to 0.4 km in width (Figs. 2A and 4B). Two large stable boulders (>1 m height) were sampled from this moraine ridge away from the hillslopes (Table 1; Fig. 3B).

4.2. Karzok study area

The Karzok study area is a broad bowl-shaped valley (~80 km^2) except for an eastern narrow outlet to Tso (Lake) Moriri (Fig. 2B). The valley is ~15-km-long and ranges between ~3 and 10 km wide. Eight small debris-free cirque glaciers are present in the valley (Fig. 2B). The youngest moraines, which are ice-contact, help form small lakes along most of these small glaciers. Moraines along Mentok Kangri to the south and Gomuche Kangri to the west of the valley were examined in this study (Figs. 2B and 4C, D).

Mentok Kangri is the largest glacier (1.5 km in length) in this study area and it extend to 5487 m asl with an ELA of ~5710 ± 30 m asl (Fig. 2B). Three sets of latero-frontal moraines are present: m_{M1}, m_{M2}, and m_{M3} (Table 1; Fig. 2B). m_{M1} is a 2.5-km-long well-preserved, steep, sharp-crested latero-frontal moraine with four recessional ice-contact ridges. The frontal section of the moraine is 300 m downstream from Mentok Kangri and rises 50 m above the present valley floor. Four boulders were sampled over its four ridges of the moraine (Table 1; Fig. 3C). Another well preserved but relatively subdued (~17-m-high) moraine, m_{M2}, is present ~380 m downstream of m_{M1} at 5350 m asl (Table 1; Fig. 4C). This latero-frontal moraine is discontinuous and consists of four ice-contact ridges over a length of 7 km. Five boulders were sampled on this moraine (Fig. 2B). Three additional boulders were also sampled from m_{M3} latero-frontal moraine, 500 m downstream of m_{M2} at 5220 m asl (Fig. 2B). This 2.4-km-long moraine consists of a single ridge with a rounded crest (Table 1).

Gomuche Kangri is the second largest glacier (~1.3-km-long) in the valley with an ELA of ~5770 ± 120 m asl that is ~270 m above the elevation of its snout (Fig. 2B). We mapped two sets of moraines, m_{G1} and m_{G2} (Table 1; Fig. 2B). m_{G1} is a 2.2-km-long latero-frontal moraine, located 220 m downstream from its snout at 5350 m asl (Fig. 4D). Three ice-contact (recessional) ridges with a mean height

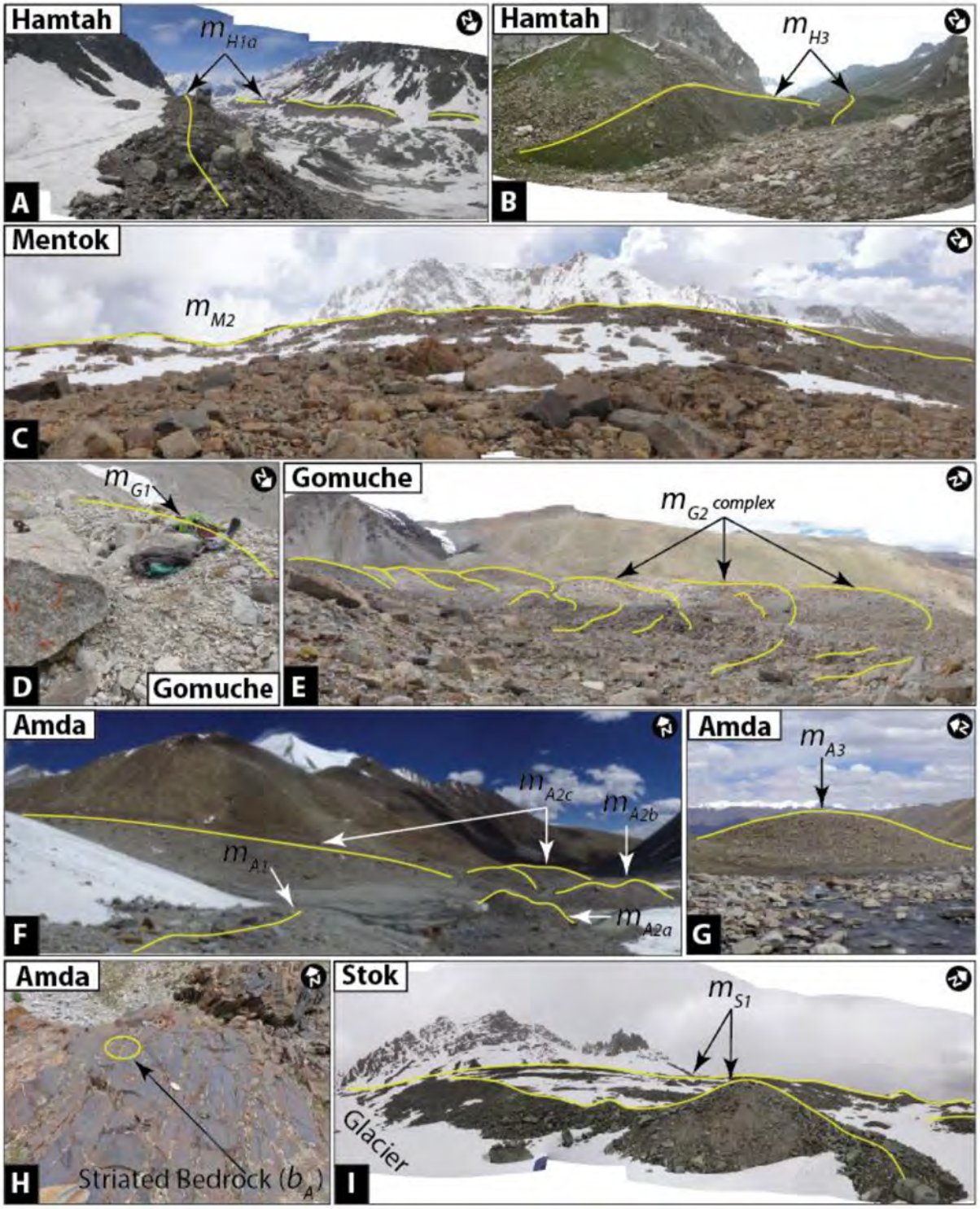

Fig. 4. Characteristics of the moraines. (A) Youngest latero-frontal moraine, m_{H1a} and (B) oldest m_{H3} lateral moraines in Hamtah valley. (C) Older Holocene m_{M2} latero-frontal moraine of Mentok Kangri in the Karzok study area. (D) Youngest m_{G1} latero-frontal moraine and (E) older m_{G2} recessional moraine complex of Gomuche Kangri in the Karzok study area. (F) Youngest moraine complex (m_{A1}, m_{A2a}, m_{A2b}, m_{A2c}) and (G) older m_{A3} end moraine of Amda Kangri in the Lato study area. (H) Striated and polished bedrock in the Lato study area. (I) Youngest m_{S1} latero-frontal moraine complex of Stok Kangri in the Stok study area. Distant and inner ridges are highlighted.

of 23 m are present above the valley floor on this moraine (Fig. 2B). Five samples were collected from the three ridges (Fig. 3D). m_{G2} consists of multiple recessional and hummocky ridges that are tens of meters long (Fig. 4E). This moraine ridge complex, extending between 5200 and 5380 m asl, is discontinuous and highly degraded, and associated with a dead-ice zone (Table 1). We sampled four boulders and additionally recalculated four published ^{10}Be ages of Hedrick et al. (2011) from the most stable three farthest recessional ridge crests (~0.3 km downstream from m_{G1}; Figs. 2B and 3E; Table 1). The ridges in the moraine complex are not well

defined and the degree of weathering is not significant enough to allow us to differentiate them into different substages.

4.3. Lato study area

The Lato study area is a ~13-km-long and ~3 km-wide valley extending between 4200 and 6200 m asl and has small debris-free glaciers in its upper reaches (Fig. 2C). The 2.9-km-long Amda Kangri and three small glaciers contribute water to the ephemeral Amda Chu that drains the valley. Amda Kangri has an ELA of ~5500 ± 20 m asl and extends to 5340 m asl. Six sets of moraines including a set of round-crested hummocky moraines are present in the valley, of which three sets of sharp-crested young moraines, m_{A1}, m_{A2} (m_{A2a}, m_{A2b}, m_{A2c}), and m_{A3} were examined in detail (Table 1; Fig. 2C). Orr et al. (2018) assigns these moraines to the Kyambu glacial stage.

m_{A1}, adjacent to the snout of Amda Kangri at 5326 m asl, is a 154-m-long and 20-m-high end moraine that trends northeast and exhibits little, if any, signs of erosion/degradation (Fig. 4F). The five granitic boulders that were sampled on the moraine were relatively stable and freshly fractured (Table 1; Fig. 3F). Two subdued recessional moraines, m_{A2a} and m_{A2b} are present at elevation of 5299 and 5298 m asl, respectively. These two moraines are inset into a 2.2-km-long north trending lateral moraine of Amda Kangri (Figs. 2C and 4F). This lateral moraine grades into a relatively well-preserved 346-m-long and 10-m-high end moraine, m_{A2c}, at 5285 m asl (Figs. 3G and 4F). We sampled six boulder samples from this ridge.

Three bedrock samples were collected from glacially sculpted striated bedrock (b_A) ~1.4 km downstream from the m_{A2c} at an elevation of 5180 m asl (Figs. 2C and 4H). A 10-m-high end moraine (m_{A3}) was also mapped and sampled some 1.6 km down the valley from glacially sculpted bedrock at 5113 m asl (Fig. 2C). This end moraine has a rounded crest with steep slopes and stretches perpendicular to the valley for a length of ~130 m (Fig. 4G). The northern part of the moraine is subdued and has subangular/subrounded denuded boulders that have undergone slight granular weathering. Many lodged striated boulders are also present on the surface of the moraine. We sampled two boulders from the southern section of the crest that consist of relatively less denuded boulders (Table 1). The northern face of the moraine is arcuate and most likely has shaped by the post-depositional river incision and/or the formation of a debris fan. A broad braided channel is developed right behind the end moraine with largely dispersed young boulders (Fig. 2C).

4.4. Stok study area

Stok Kangri and four debris-free cirque glaciers are present in the upper reach of the Stok valley (Fig. 2D). This sub-polar type glacier is 1.8 km long with an ELA of ~5480 ± 30 m asl. Building on the work of Orr et al. (2017), we recognize four sets of moraines in the upper Stok valley: m_{S1}, m_{S2}, m_{S3}, m_{S4}, and m_{S5} (Table 1; Fig. 2D). For our study, we have only targeted the m_{S1} moraine complex for dating (Fig. 2D). Orr et al. (2017) discusses the discrepancies between the exposure ages of the moraine complex and their morphostratigraphic contexts. The southern latero-frontal ridges (their M_{S2}) are interpreted as older than northern latero-frontal ridges (their M_{S1}) of m_{S1} moraine complex. Our new study updates the field map and morphostratigraphic interpretation presented in Orr et al. (2017).

The m_{S1} moraine complex is at ~5230–5450 m asl (Fig. 2D) and is composed of diamicton containing highly fractured boulders and cobbles supported by a coarse gravel-sandy matrix (Table 1). The southern latero-frontal moraine of m_{S1} has a length of ~1.5 km and consists of >4 recessional ridges, whereas the northern latero-frontal moraine is ~1.3-km-long and consist of ~3 inner recessional ridges (Fig. 2D). The mean relief of these ridges is similar (~30 m high) (Fig. 2D). Four boulder samples (STOK-1401 to 1404) were collected by Orr et al. (2017) from the distant ridge of the north latero-frontal moraine (Fig. 4I), and five samples including a new one (STOK-1405 to 1408 and 1516) were collected from the inner ridges of the south latero-frontal moraine (Fig. 2D). The distant ridge of north latero-frontal moraine also consists of more weathered boulders (Table 1). Based on its morphostratigraphic position and relative weathering, we reinterpreted the distant northern ridge (M_{S1} of Orr et al., 2017) of the moraine complex to be older than inner southern ridges (M_{S2} of Orr et al., 2017). A summary of characteristics of all moraines, bedrock, and sampled boulders in our study areas are provided in Table 1.

5. Dating results

5.1. Hamtah study area

m_{H3} is correlated with Kulti glacial stage moraines of Owen et al. (1996, 1997, 2001) in Lahul. Ages for m_{H3} range from ~16.2 to 4.0 ka (χ^2 value of 98.3; Fig. 5A; Table 2). Three outliers (Hamtah 1402, 1403, and 1404) were identified and discarded from the final analysis (Table 2; Fig. 5A). The remaining three samples have a weighted mean age of 10.4 ± 0.4 ka (Table 4; Fig. 6A). This early Holocene glacier advance overlaps (at ±2σ) with the previously reported Kulti glacial stage of Owen et al. (2001) at 11.6 ± 0.6 ka in the Chandra valley, Lahul (n = 2; recalculated here in Supplementary material S3). However, using different *in situ* ^{10}Be production rates Eugster et al. (2016) assigned the Kulti glacial stage to 13.7 ± 1.3 ka.

Ages for m_{H1a} range from ~2.4 to 0.14 ka (Fig. 5B; Table 2) with a high degree of dispersion (i.e., χ^2 is 124.9; Fig. 6B). Since most of the samples were collected away from slope deposits and they show no sign of post-depositional modification, one possibility is that the age range is due to varying prior-exposure histories. The skewed distribution toward the younger ages (skewed +2.13) further suggests that the older ages are due to inherited ^{10}Be (Ivy-Ochs et al., 2007). Although, we have assumed no production of ^{10}Be during glacial transport, a horizontal surface flow velocity of ~20–14 m yr^{-1} (Shukla et al., 2015) could account for inheritance of as much as ~0.3–0.1 ka. Two outliers (Hamtah 1408 and 1502 in Table 2) were identified and removed, leaving an age range of ~0.4 to 0.1 ka. The tentative weighted mean moraine age based on three boulders is ~0.2 ± 0.1 ka (Table 4; Fig. 6B).

5.2. Karzok study area

Ages for m_{M3} range from ~57.2 to 22.9 ka with a χ^2 value of 124.0 (Fig. 5C; Table 2). Since, most of the granitic boulders on this moraine exhibit spheroidal weathering, the ages may be affected by post-depositional modification of the boulders (Supplementary material S2). We tentatively associate the moraine age with oldest boulder age (57.2 ± 3.5 ka).

m_{M2} has five ages that are similar except for one outlier, KO-1 (Fig. 5C, Table 2). The outlier-free distribution yields a weighted mean age of 1.0 ± 0.1 ka (Table 4; Fig. 6C). These ages are similar across all the four ice-contact ridges of m_{M2} moraine, which suggests that all the moraine ridges may have all formed within several decades.

Four ages for m_{M1} are tightly clustered, except for one outlier, KO-7 at ~0.2 ka (Fig. 5C; Table 2). After eliminating the outlier, the moraine has a weighted mean age of 0.7 ± 0.1 ka (Table 4; Fig. 6D).

The four ages for m_{G2} when combined with four additional ages from Hedrick et al. (2011) range from ~23 to 3.3 ka (χ^2 = 111.3;

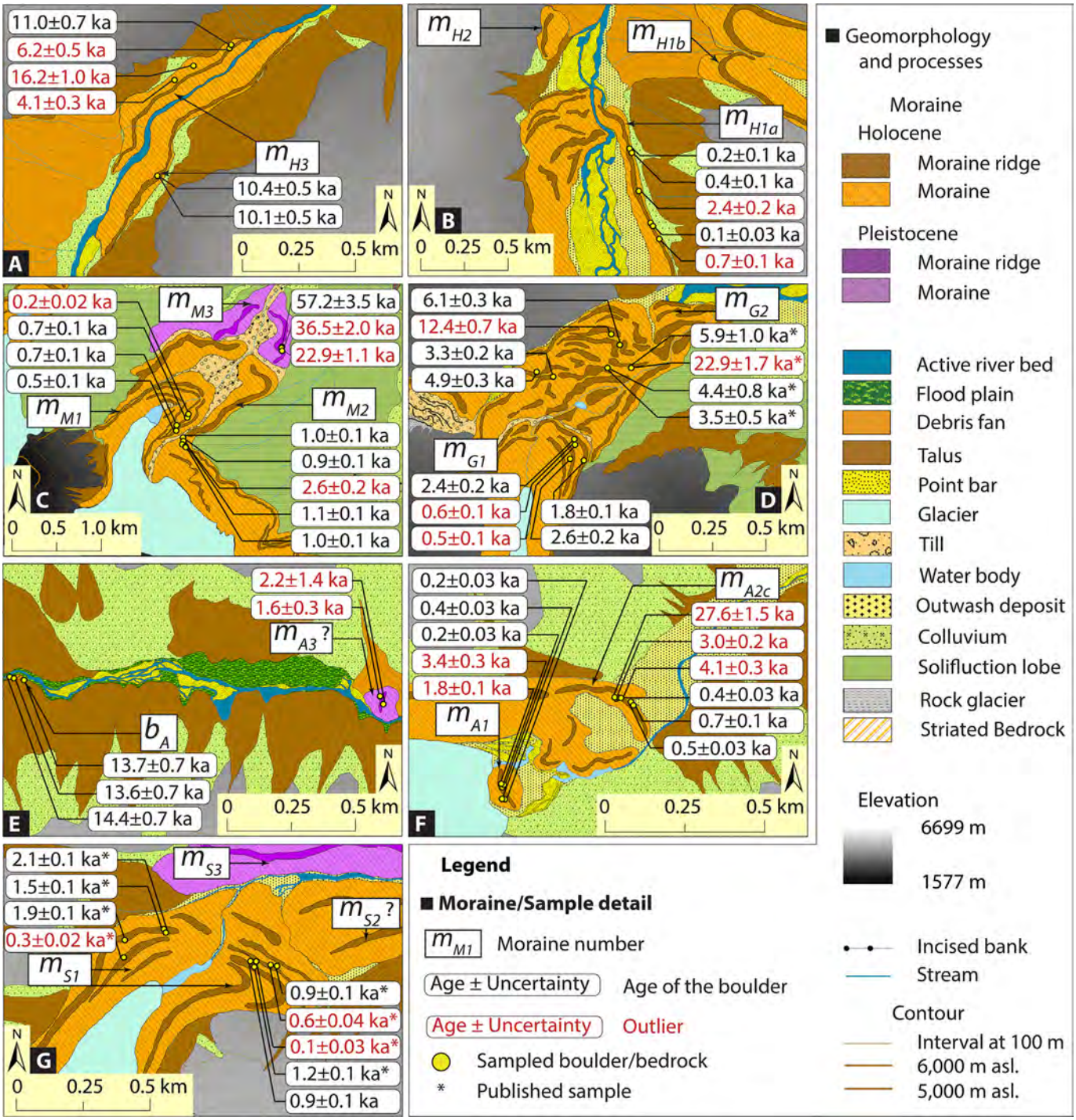

Fig. 5. Geomorphology of the study areas with cosmogenic ^{10}Be surface exposure ages. (A) Enlarged Hamtah valley showing the ^{10}Be ages on the oldest (m_{H3}) and (B) youngest (m_{H1a}) moraines. (C) Mentok Kangri with ^{10}Be ages. (D) Gomuche Kangri with new and published ^{10}Be ages (*). (E) Enlarged section of the Amda Kangri showing oldest moraine, m_{A3}, and bedrock samples with ^{10}Be ages shown in boxes and (F) youngest moraine (m_{A1}) showing ^{10}Be ages. (G) Stok moraine complex (m_{S1}) with ^{10}Be ages. Note that the maps are based on UTM projection (Zone 43N) and WGS 1984 datum. See online version of the figure for more clarity.

Fig. 5D; Table 2). Two outliers are evident (KO 1502: 12.4 ± 0.7 ka and TM-C: 22.9 ± 1.7 ka). After omitting the outliers, the remaining six ages have an overlapping multimodal normal kernel density distribution (Fig. 6E). m_{G2} appeared to be a detached dead-ice section of the main glacier which was likely unstable during the past (Fig. 4E). Some of the young ages are possibly the result of post-depositional toppling of moraine boulders. It is not possible to assign a mean age to this moraine with confidence, but we suggest that this moraine likely formed between ~6.1 and 3.3 ka (Table 4; Fig. 6E).

The five ages for m_{G1} range from ~2.6 to 0.5 ka with a χ^2 value of 181.7 (Fig. 5D; Table 2). Two young outliers (KO 15 at ~0.6 ka and KO16 at ~0.5 ka), which are morphostratigraphiclly inconsistent (Fig. 5D), were omitted (Fig. 6F, Table 2). Field observations of the sampled boulders (Supplementary material S2) indicates that they are inset a little off-the-crest of the moraine. It is highly possible

Table 4
A summary of Holocene local and regional stages of glacier advances based on cosmogenic ^{10}Be surface exposure age data.

Regional glacial stage	Local glacial stage	Local stage age (ka)[a]	Regional stage age range (ka)	n (outlier free)	Chi-squared value [b]	Mean regional glacial stage age (ka)[c]	P $_{(sig\ 2\text{-}tailed)}$ between regional glacial stages
HH 7	m_{H3} (This study)	10.42 ± 0.34	~10.9–9.3	3	0.48	10.06 ± 0.42	0.000
	Olimde 3 stage (Seong et al., 2009)	10.25 ± 0.15		6	0.10		
	Olimde 3 stage (Seong et al., 2009)	9.80 ± 0.32		8	0.43		
HH 6	Olimde 4 Stage (Seong et al., 2009)	7.98 ± 0.09	~8.2–7.4	6	0.06	7.83 ± 0.23	0.004
	Olimde 4 Stage (Seong et al., 2009)	7.77 ± 0.26		5	0.48		
	Olimde 4 Stage (Seong et al., 2009)	7.74 ± 0.24		6	0.41		
HH 5	Mungo 2 stage (Seong et al., 2007)	6.63 ± 0.30	~6.9–4.3	4	0.68	5.13 ± 1.11	0.000
	Askole 2 stage (Seong et al., 2007)	5.83 ± 0.60		4	0.92		
	Olimde 5 stage (Seong et al., 2009)	5.06 ± 0.12		3	0.33		
	KM-4 stage/m_{G2} (Hedrick et al., 2011; This study)	4.94 ± 0.28		6	13.12		
HH 4	Olimde 6 stage (Seong et al., 2009)	4.32 ± 0.09	~4.5–2.8	3	0.19	3.87 ± 0.58	0.000
	Olimde 6 stage (Seong et al., 2009)	3.95 ± 0.25		3	2.17		
	PM-2 stage (Hedrick et al., 2011)	3.42 ± 0.71		3	17.79		
HH 3	Ladakh Chang La cirque (Dortch et al., 2013)	2.31 ± 0.24	~2.7–1.8	4	2.01	2.19 ± 0.22	0.000
	Olimde 7 stage (Seong et al., 2009)	2.19 ± 0.07		6	0.19		
	m_{G1} (This study)	2.10 ± 0.34		3	9.37		
HH 2	m_{S1} (This study)	1.20 ± 0.05	~1.8–0.9	6	21.83	1.15 ± 0.39	0.000
	Olimde 7 stage (Seong et al., 2009)	1.66 ± 0.14		3	0.75		
	Olimde 7 stage (Seong et al., 2009)	1.35 ± 0.36		4	4.58		
	m_{G1} (Orr et al., 2017)	1.33 ± 0.12		1	?		
	Askole 3 stage (Seong et al., 2007)	1.03 ± 0.28		5	0.82		
	m_{M2} (This study)	0.99 ± 0.07		4	0.90		
HH 1	m_{M1} (This study)	0.67 ± 0.07	<1 ka	3	1.47	0.37 ± 0.20	0.000
	Olimde 8 stage (Seong et al., 2009)	0.66 ± 0.22		3	10.19		
	Upper Yunam (Saha et al., 2016)	0.59 ± 0.11		3	2.13		
	Pangong high cirque (Dortch et al., 2013)	0.50 ± 0.09		3	0.63		
	Olimde 8 stage (Seong et al., 2009)	0.48 ± 0.13		4	4.19		
	Lonp stage (Lee et al., 2014)	0.47 ± 0.10		2	12.53		
	m_{A2c} (This study)	0.45 ± 0.16		3	24.25		
	m_{A1} (This study)	0.26 ± 0.06		3	6.78		
	PM-3 stage (Hedrick et al., 2011)	0.26 ± 0.04		3	2.22		
	m_{H1a} (This study)	0.18 ± 0.11		3	8.55		

[a] All local stage age uncertainties are reported in 1σ.
[b] Corrected Chi-squared values are from outlier free distribution.
[c] All regional stage age uncertainties are reported in 1σ.

that this moraine is unstable and post depositional toppling of some boulders may have occurred. Due to the smaller length of the glacier (~1.3 km), inherited ^{10}Be production during transport is probably less (>0.2 ka; assuming horizontal surface flow velocity of the glacier is 7–4 m yr^{-1} after Scherler et al., 2011) than the uncertainty of moraine formation. We tentatively assign a weighted mean age of 2.1 ± 0.4 ka to this moraine (n = 3; Table 4; Fig. 6F).

5.3. Lato study area

The older moraine, m_{A3}, has young exposure ages (2.1 ± 1.4 and 1.6 ± 0.3 ka). These ages are also reported in Orr et al. (2018) and they have assigned these moraine ages to their Kyambu glacial stage. However, these ages are morphostratigraphically inconsistent and have very high uncertainties (>66%). The moraine should be much older than the bedrock ages (b_A: ~14 ka) sampled further upstream from this moraine (Fig. 5E; Table 2). Since, we preferentially sampled larger fresh boulders from the southern face of the moraine, that appears overridden by recent hillslope deposits, one possibility is that we may have sampled boulders deposited much later than the stabilization of the moraine and hence may represent hillslope activity than the absolute age of the moraine. We are unable to assign a numerical age to this moraine.

The three bedrock ages for b_A are consistent (Fig. 5E; Table 2) and have a weighted mean age of 13.9 ± 0.4 ka (Fig. 6G).

The ages for m_{A2c} range from ~27.6 to 0.4 ka (Fig. 5F; Table 2). Even after three outliers (Lato 1409, 1410, and 1411) were omitted from the age distribution, the dispersion is still high with a χ^2 value of 24.3 (Fig. 6H). There was no sign of differential surface erosion and/or post depositional modification of these boulders and the surface of the moraine ridge is stable with a rounded crest. While it is possible that two older age outliers (~4 and ~3 ka) from m_{A2c} may have undergone different prior-exposure histories in this low erosion rate setting, the possibility of boulder toppling is very unlikely (Supplementary material S2). We therefore, discarded the two outliers (Table 2) and the outlier free population ranges between ~0.7 and ~0.4 ka with a tentative weighted mean moraine age of 0.5 ± 0.2 ka (Table 4; Fig. 6H).

Five ages for m_{A1} range from ~3.4 to 0.2 ka (Fig. 5F; Table 2). After omitting two older outliers (Lato 1415 at ~1.8 and LATO 1419 at ~3.4 ka), we assign a weighted mean age of 0.3 ± 0.1 ka to this moraine (Table 4; Fig. 6I).

5.4. Stok study area

Four ages for the distant northern ridge of m_{S1} that were determined by Orr et al. (2017) range from ~2.1 to 0.3 ka, whereas five ages for the southern moraine, that include one new and four previously published ages in Orr et al. (2017), range between ~0.9 and ~0.1 ka (Fig. 5G; Table 2). A young outlier (Stok 1404 with an age of ~0.3 ka) from the northern latero-frontal moraine and two young outliers (Stok 1406 and 1407 at ~0.6 and ~0.1 ka, respectively) from the southern latero-frontal moraine are evident and excluded from the subsequent analysis (Table 2). Field evidence

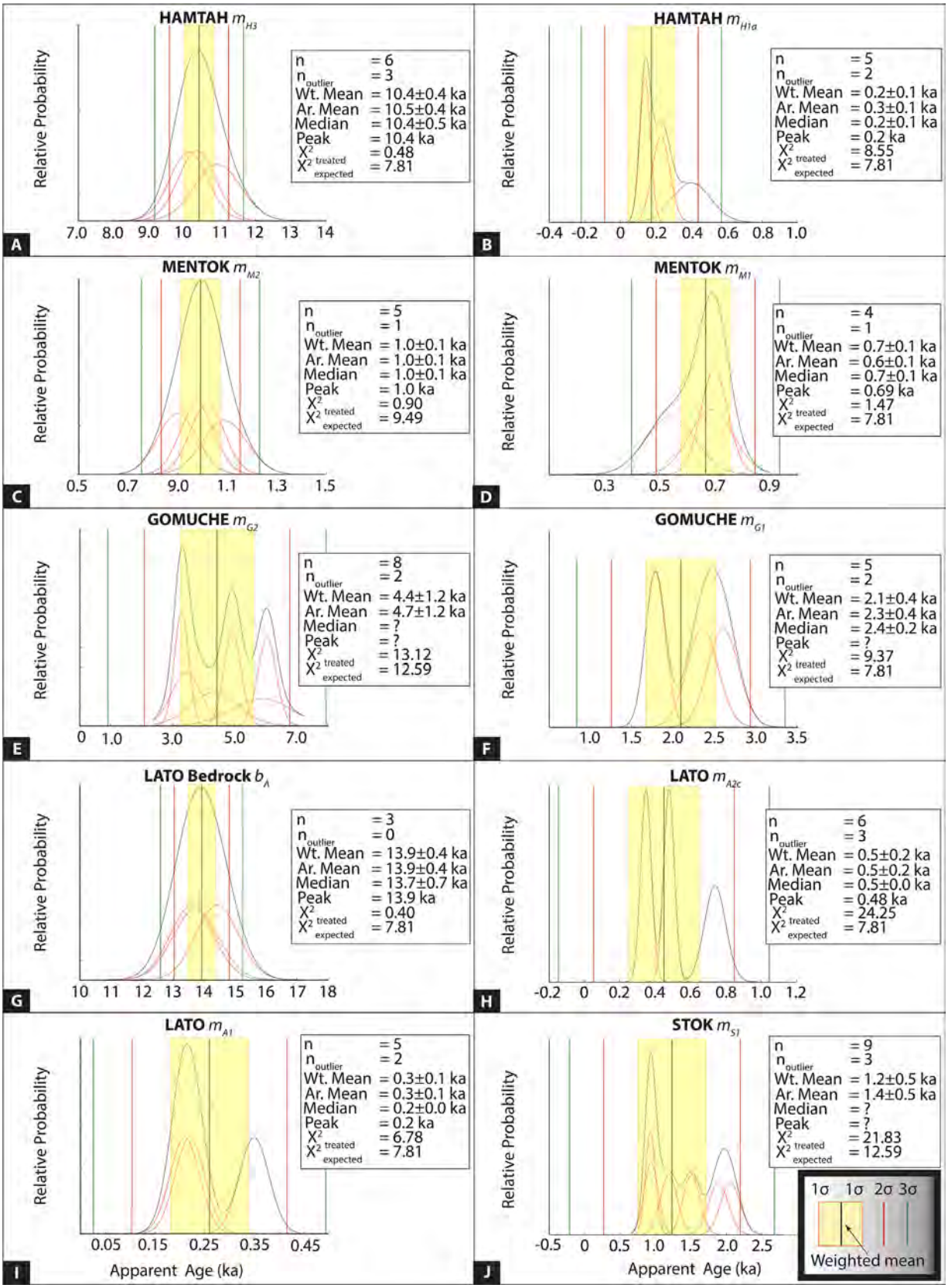

Fig. 6. Probability density plots showing outlier-free age distributions for each dated moraine in the study areas. Relevant age statistics are enclosed in boxes of each members. Age uncertainties (1σ, 2σ, and 3σ) are represented by vertical lines. This statistical treatment proved robust for moraines with χ^2 of outlier-free population (called here as $\chi^2_{treated}$) within expected 95% confidence interval of a normal kernel density functions (which we called $\chi^2_{expected}$). The moraines with $\chi^2_{treated} > \chi^2_{expected}$ are interpreted as tentative (lower confidence) in this study.

(see Supplementary material S2) suggests possible toppling and displacement (i.e., incomplete exposures) of these young outlier samples. The recessional moraine ridges of m_{S1} also appeared unstable at several places. Although we avoided sampling unstable locations, the stability of the moraine complex in the recent past is not entirely clear. In contrast to boulder toppling, an inherited ^{10}Be concentration during supraglacial transport may result in age overestimation by ~0.3–0.1 ka (assuming the same glacier surface velocity as Gomuche Kangri). Similarly, since some of the older age boulders at the northern ridge are close to cirque walls (Fig. 4I), they are likely to be affected by reworking and hillslope deposits and therefore, may be biased by inheritance. The outlier free distribution shows overlapping multimodal relative probabilities (Table 4; Fig. 6J), thus we refrain from assigning any mean age to this moraine complex; its age is likely bracketed between ~2.1 and ~0.9 ka (Table 4; Fig. 6J).

6. Equilibrium-line altitudes

The reconstructed steady-state ELAs for our study areas, in general, reflect gradual altitudinal rise of ~180–4 m since the early Holocene in the Lahul and the Zanskar study areas. Hamtah glacier in Lahul was the most extensive (~10.7 km long) during the early Holocene at ~10.4 ka with ΔELA of ~182 ± 57 m (Table 5). The next dated glacier advance, at ~0.2 ka, had a ΔELA of ~57 ± 28 m (Table 5).

In the Karzok valley, Gomuche Kangri experienced relatively larger (extending ~0.8 km) Neoglacial glacier advances during ~6.1–3.3 ka, with a ΔELA of ~159 ± 77 m. The ΔELA was ~64 ± 50 m during a later restricted advance (extending ~0.2 km) at ~2.1 ka (Table 5). The adjacent Mentok Kangri, however, only extended ~0.5 and 0.3 km during the late Holocene, at ~1.0 and ~0.7 ka, with ΔELAs of ~63 ± 6 and 21 ± 3 m, respectively (Table 5).

In the Lato valley, Amda Kangri advanced at ~0.5 and ~0.3 ka and was restricted to ~0.4 km (ΔELAs of ~21 ± 7) and ~0.04 km (ΔELAs of ~4 ± 4 m) from its contemporary glacier terminus, respectively (Table 5).

The late Holocene moraine complex (m_{s1} at ~2.1–0.9 ka) of the Stok Kangri represents a glacier advance of ~0.3 km from its contemporary terminus, with a ΔELAs of ~65 ± 11 m (Table 5).

7. Discussion

7.1. Local glacial stages in study areas

The young moraines in our study exhibit scattering in ^{10}Be ages (16 outliers out of 49; Fig. 7A; Table 2). These scattering manifests themselves in χ^2 of >1, positive skewness, and convex upward cumulative probability density distributions (cf. Applegate et al., 2012). Our interpretation of the cosmogenic ^{10}Be measurements is that for especially young features, i.e. Holocene, inherited ^{10}Be could represent a substantial fraction of the cosmogenic ^{10}Be inventory. Likewise, the instability of many of the sample surfaces increases the possibility that some samples have not been exposed to cosmic rays continuously since the deposition time of the surface. Since, most of the glaciers in our study are cold-based subpolar types that are not substantially erosive in nature (except Hamtah glacier), the limited erosion of bedrock cliffs (>0.6 m of bedrock erosion is required to obtain rock with no ^{10}Be) that overhang these glaciers, and/or reworking of older glacial deposits, could help explain the presence of inheritance (cf. Applegate et al., 2012). An additional complication is the possibility of ^{10}Be production in boulders *en transit* to deposition. Supraglacial exposure might lead to an overestimate of moraine ages by as much as ~0.3–0.1 ka as well as adding scatter. Recent studies which date supraglacial boulders on glacier surfaces (cf. Ward and Anderson, 2011), suggest age inheritance ranging between ~0.9 and ~0.05 ka for more humid glaciers in the Central and Eastern Himalaya

Table 5
A summary of ELAs and ΔELAs in our four study areas.

Glacial Stage	Mean moraine age (ka)	Glacier area (~km2)	Mean slope (°)	Mean Aspect	Head (m asl)	Toe (m asl)	MELM (m asl)	Area-Altitude	Area-Accumulation ratio			Toe-Headwall altitude ratio			Mean ELA (m asl)	ΔELA (m)
								AA (m asl)	AAR (0.5)	AAR (0.6)	AAR (0.7)	THAR (0.3)	THAR (0.4)	THAR (0.5)		
Hamtah Valley, Lahul																
Present		4.0	27	NW	5011	4056	4569	4459	4479	4429	4380	4347	4443	4540	4456 ± 70	
m_{H1a}	0.18 ± 0.13	5.6	29	NW	5063	3941	–	4407	4429	4389	4259	4285	4397	4510	4382 ± 79	57 ± 28
m_{H3}	10.42 ± 0.42	6.6	30	NNW	5063	3688	–	4332	4389	4240	4119	4103	4241	4380	4258 ± 108	182 ± 57
Mentok Kangri, Karzok																
Present		2.5	33	NE	6003	5482	5659	5740	5739	5719	5689	–	–	–	5709 ± 31	
m_{M1}	0.67 ± 0.09	2.8	34	NE	6003	5447	–	5714	5720	5699	5669	–	–	–	5701 ± 20	21 ± 3
m_{M2}	0.99 ± 0.08	4.1	30	NE	6003	5378	–	5685	5679	5650	5620	5568	5631	5695	5647 ± 41	63 ± 6
Gomuche Kangri, Karzok																
Present		1.5	42	N	6084	5381	5649	5873	5929	5889	5839	5599	5669	5740	5773 ± 117	
m_{G1}	2.10 ± 0.42	1.8	42	N	6084	5332	–	5805	5889	5819	5660	5564	5639	5715	5727 ± 107	64 ± 50
m_{G2} (or KM-4)	4.40 ± 1.17	2.1	39	NNE	6084	5206	–	5732	5829	5649	5530	5473	5561	5650	5632 ± 113	159 ± 77
Amda Kangri, Lato																
Present		1.1	22	ENE	5743	5312	5489	5538	5529	5509	5469	–	–	–	5504 ± 24	
m_{A1}	0.26 ± 0.08	1.4	25	ENE	5764	5298	–	5533	5529	5499	5469	–	–	–	5511 ± 27	4 ± 4
m_{A2c}	0.45 ± 0.02	1.6	25	ENE	5764	5264	–	5511	5519	5479	5439	–	–	–	5487 ± 31	21 ± 7
Stok Kangri, Zanskar																
Present		0.6	36	NE	5721	5288	5459	5507	5509	5489	5439	–	–	–	5481 ± 27	
m_{S1}	1.20 ± 0.48	0.9	34	NE	5748	5234	–	5456	5439	5409	5379	–	–	–	5421 ± 29	65 ± 11

Note: The present here refers to year 2016 AD.
m asl is meter above sea level.
'-' indicates reconstructed ELAs are ambiguous/erroneous.

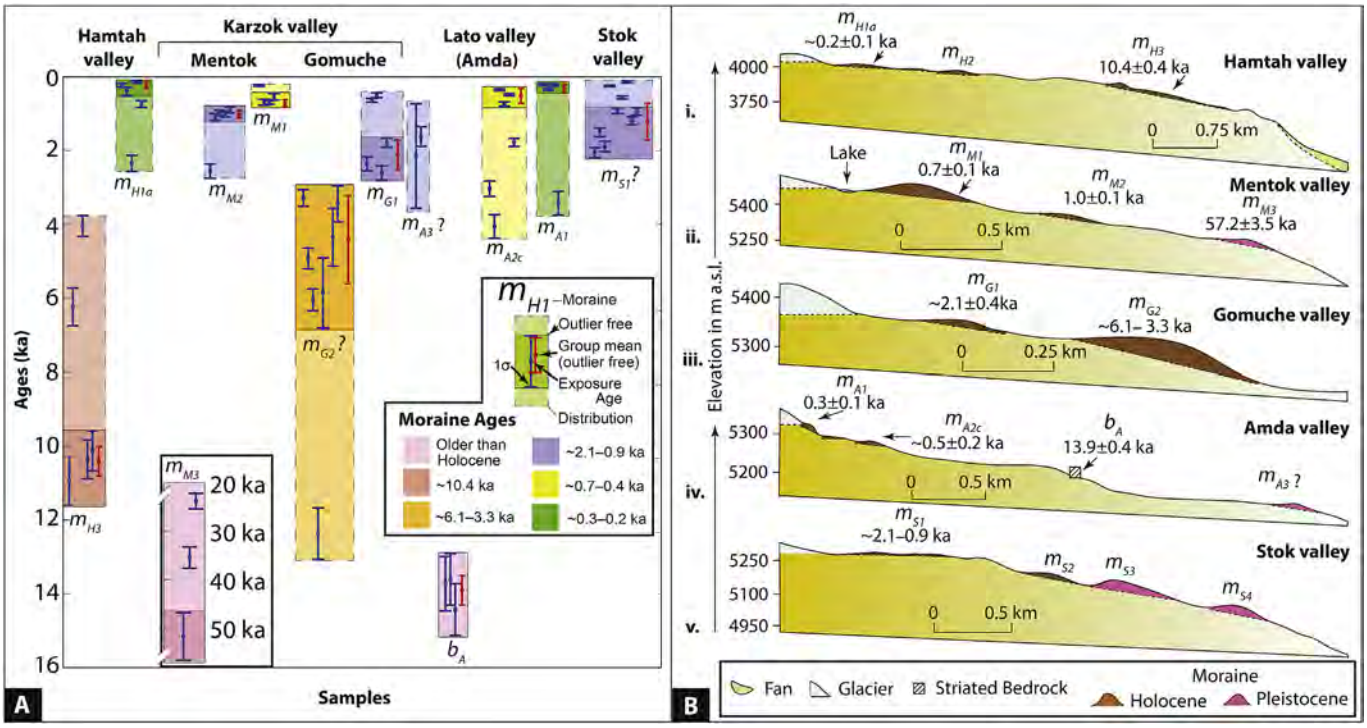

Fig. 7. ^{10}Be ages for new study areas. (A) Scatter plot with error bars showing local glacial stages from four study areas. Moraine boulder ages are arranged by morphostratigraphy from oldest to youngest for each valley. (B) Schematic longitudinal topographical profiles of each of the studied glaciated valley with their (weighted) mean±1σ moraine exposure ages.

(Heimsath and McGlynn, 2008; Murari et al., 2014). Post-depositional boulder toppling could also contribute to scatter by exposing fresh surfaces after deposition of the moraine. These processes are likely present in all glacial settings, but for LGM or older features the production of ^{10}Be in supraglacial boulders or the toppling of a boulder in the first ~1 ka of a moraine represents an undetectable perturbation on the ^{10}Be inventory. For Holocene glaciation the impact of these processes is potentially substantial and may be a major contributor to scatter in our results (Supplementary materials S3). The m_{S1} complex in Stok Kangri supports the view that instability and possible post-depositional boulder toppling (incomplete-exposures) may contribute to spread of ^{10}Be ages on moraines. Post-depositional hillslope contamination, e.g., supply of rock fall debris to moraines, however, is a possibility for age scatter for the m_{H3} in Hamtah and m_{A3} in Lato (Supplementary materials S8).

Despite the scatter introduced by these geologic factors, we identify five Holocene local glacial stages using the 49 new and 12 published (Hedrick et al., 2011; Orr et al., 2017) ^{10}Be ages. These date to ~10.4, ~6.1–3.3, ~2.1–0.9, ~0.7–0.4, and ~0.3–0.2 ka, with three synchronous advances at ~2.1–0.9, ~0.7–0.4, and ~0.3–0.2 ka (Table 4; Fig. 7A).

A large glacier advance occurred in the early Holocene in the Hamtah study area, which is the wettest (~800–400 mm) of our study areas. Hamtah glacier extended >10 km in Lahul at ~10.4 ka (Fig. 7A, Bi) with an ΔELA of ~182 ± 57 m (Tables 4 and 5). Similar extensive early Holocene local glacial stages are evident in the semi-arid Muztag Ata-Kong Shan region of the northwestern Tibet (Seong et al., 2009), but with larger ΔELAs of between ~797 ± 129 and 574 ± 181 m (Supplementary materials S7, S9).

Neoglacial glacier advances at ~6.1–3.3 and ~2.1–0.9 ka in our semi-arid study areas of the Zanskar Range were restricted in extent (<1.0 km; Fig. 7A, Biii; Table 4). Gomuche Kangri in the Karzok valley advanced ~0.8 km (~159 ± 77 m) at ~6.1–3.3 ka; we cannot assign a precise age to this glacier advance. Coeval local glacial advances also occurred in other areas of Zanskar, e.g., in the Puga valley (Hedrick et al., 2011), in the mid-latitude westerlies dominated Central Karakoram (Seong et al., 2007), and in semi-arid Muztag Ata (Seong et al., 2009), with ΔELAs ranging from ~650 to 150 m (Supplementary materials S7, S9).

Restricted (~0.3 km) local glacier advances at ~2.1 ka occurred in the Karzok valley (Fig. 7A, Biii), Ladakh (Dortch et al., 2013) and in Muztag Ata (Seong et al., 2009), with a ΔELAs ranging between ~130 and 56 m (Supplementary materials S3, S7). An equally restricted glacier advance (~0.3 km) occurred at ~2.1 to 0.9 ka in the Stok valley (Fig. 7A, Bv). We are unable to assign a precise age to this local glacier advance. Another restricted (~0.5 km) local glacier advance at ~1.0 ka occurred in the Mentok Kangri valley, with a ΔELA of ~63 ± 6 m (Fig. 7A, Bii). Corresponding glacier advances are also proposed for the Central Karakoram and northwestern Tibet at between ~1.7 and 1.1 and ~1.0–0.9 ka, respectively (Supplementary material S3 and references therein).

Two local glacial stages with limited extent (<0.4 km) occurred during the late Holocene, at ~0.7–0.4 ka in the Karzok and Lato study areas (Fig. 7A, Bii, Biv) and at ~0.3–0.2 ka in the Hamtah and Lato study areas (Fig. 7A, Bi, Biv). These local glacial stages probably represent Little Ice Age (LIA) glacier advances with ΔELAs ranging between ~57 and ~4 m (Supplementary materials S7, S9). Coeval LIA stages are also recognized in the other valleys in Zanskar (Hedrick et al., 2011; Dortch et al., 2013; Saha et al., 2016), Ladakh (Lee et al., 2014), and in Mustag Ata (Seong et al., 2007, 2009; Supplementary material S3).

7.2. Himalayan Holocene regional glacial stages (HH)

We propose seven Himalayan Holocene regional glacial stages

(HHs) using our 49 new and 187 published ^{10}Be ages from a total 32 glaciated valleys across the northwestern end of the Himalaya and Tibet (Figs. 8 and 9; Table 4; Supplementary material S3). The modern distribution of moraine successions is being utilized as proxy for paleoclimate (e.g., Benn and Ballantyne, 2005; Ballantyne et al., 2007; Owen and Dortch, 2014), but this approach has been questioned because several additional non-climatic factors are also believed to influence moraine formation (Warren and Hulton, 1990; Kaplan et al., 2009; Roe and O'Neal, 2009; Roe, 2011; Anderson et al., 2012; Barr and Clark, 2012; Barr and Lovell, 2014) and their preservation (Putkonen and O'Neal, 2006; Kirkbride and Winkler, 2012). These factors include: moraines formed by valley glaciers that are significantly impacted by topography (Barr and Lovell, 2014); micro-climate (Oerlemans, 2010); glacier response time (Oerlemans, 2005); erosional censoring (Kirkbride and Winkler, 2012); altered glacier flow by the presence of pre-exiting landforms/deposits (Owen et al., 2001); and intrinsic climate variability (Roe and O'Neal, 2009; Roe, 2011).

While these non-climatic geologic factors undoubtedly impact glacial activity, they may have only a limited effect on Holocene timescales. For instance, erosion censoring (or eradication) of geomorphic records and self-defeating feedback mechanisms (see Macgregor et al., 2000; Kaplan et al., 2009) are unlikely since we use mostly small cirque and valley glaciers in relatively semi-arid/arid climate (except transitional climate in Hamtah valley) in our study. The progressively decreasing extent of glacier advances over the Holocene are least likely to be modified by erosional feedback mechanisms (see Barr and Lovell, 2014). Limited range-scale uplift (<20 m in 10 ka after Lavé and Avouac, 2001) during the Holocene makes it unlikely that any significant topographic/tectonic controls have occurred (see Barr and Lovell, 2014). However, a complex combination of other stochastic factors specific to each locality, including climatic and microclimatic regimes, climate variability, pre-existing topography, debris cover, glacial history, and geologic setting, could influence the timing and extent of Holocene glaciation and the preservation of glacial evidence in our study areas (Hobley et al., 2010; Dortch et al., 2011; Dietsch et al., 2015).

Despite these limitations, glacial chronologies represent a significant archive of climate and considerable effort continues to be made to link timing and extent of past glacier advances (Gillespie et al., 2003; Grove, 2008; Davis et al., 2009; Dortch et al., 2013) to climate change (Dyke and Savelle, 2000; Putnam et al., 2013b), including ELA reconstructions (Benn and Lehmkuhl, 2000; Kaplan et al., 2013). Reconstructing regional glacial stages based on multiple local stages, thus provide an opportunity to address these issues and the large-scale assessment of glaciation, which may differ locally. In our study, a regional assessment helps us to compare changes in ELAs between more monsoonal glaciers to the south and more arid sub-polar type glaciers to the north (Supplementary material S9). The glaciers in the south are more sensitive to changes in temperature and therefore, likely more extensive during colder events. The opposite is true for the more cold-based glaciers in the northern regions, which are more sensitive to changes in moisture supply (Benn and Owen, 2002).

Each HH is discussed below and broad-scale possible forcing factors for glaciation are considered (Fig. 8). However, correlating discrete glacial records with continuous climate proxy records is challenging and should be interpreted cautiously (see Roe, 2011). Here, we speculate on possible climate forcing by considering the high-resolution proxy records as a guide to assess climatic integrity, spatial coherence, and chronological robustness of our HHs, as generally proposed by Kirkbride and Winkler (2012).

7.2.1. Regional glacial stages for the late glacial

Two late glacial regional glacial stages, i.e., ~15.4–12.7 and ~12.6–11.4 ka, are evident in our analysis (Figs. 8A and 9; Supplementary material S3). These late glacial advances often extend into the Holocene and are also crucial to understand the long-term possible forcing factors. The weighted means of these glacier advances are at 13.9 ± 0.7 and 11.9 ± 0.5 ka.

Our limited analysis of ΔELAs in thirteen glaciated valleys broadly indicates extensive glacier advances during ~15.4–12.7 ka in the Central Karakoram (except in the Hunza valley) and Muztag Ata (~1105–491 m). In comparison, temperate glaciers in Lahul to the south are relatively restricted (ΔELA ~490–340 m), possibly indicating enhanced moisture supply further north. Moisture supply may be orographically restricted (ΔELA ~122–97 m) in the Pamir and Alay Ranges during these glacier advances, which is in the extreme northwest of our study areas (see Supplementary materials S9). We speculate that these glacial advances may be coeval with the enhanced monsoon in the orogen during Bølling-Allerød Interstadial (~14.7–12.7 ka; Fig. 9).

Glacier advances are also dated during ~12.6–11.4 ka in Lahul, Central Karakoram, and Muztag Ata. Relatively larger ΔELAs are evident for Lahul and Central Karakoram (~580–667 m) compared to those in the Muztag Ata-Kong Shan region (~201 ± 117 m) (see Supplementary materials S9). However, our data is too limited to confirm any climatic influence during this stage. We speculate that the timing of this glacier advance might be coincident with the Younger Dryas (YD) Stadial (12.9–11.7 ka) and North Atlantic cooling (Denton and Broecker, 2008; Chiang et al., 2014).

These glacier advances closely match with the proposed semi-arid western Himalayan-Tibetan stages (SWHTS) 2B (13.9 ± 0.5 ka) and 2A (12.2 ± 0.8 ka) of Dortch et al. (2013) and the monsoonal Himalayan-Tibetan stages (MOHITS) 2A (12.9 ± 0.9 ka) and 1K (11.4 ± 0.7 ka) of Murari et al. (2014 and references therein).

7.2.2. HH 7 (~10.9–9.3 ka)

A short-term but relatively extensive early Holocene glacier advance is recognized from three local glacial stages with ages ranging from ~10.9 to 9.3 ka and a weighted mean of 10.1 ± 0.4 ka, which we call HH 7 (Figs. 8A and 9; Table 4). This regional glacial chronostratigraphy matches closely with the MOHITS 1J at 10.1 ± 0.5 ka of Murari et al. (2014 and references therein) for the monsoonal eastern and central Himalaya. Larger changes in ELAs (~797–574 m) are evident in northern sub-polar glaciers in Muztag Ata (Seong et al., 2009) than in southern temperate/monsoonal glaciers in Lahul (~182 ± 57 m; see Supplementary materials S9). We speculate, given dataset size, that this is largely because of relatively enhanced moisture supply and associated cloud albedo and radiative cooling in the cold-based northwestern Tibetan glaciers (cf., Rupper et al., 2009). The onset and rapid increase in monsoonal precipitation following a northerly shift of the Intertropical Convergence Zone (ITCZ) is also widely suggested during this time on the basis of speleothem (Fleitmann et al., 2003, 2007; Dykoski et al., 2005; Wang et al., 2005; Hu et al., 2008), and glacial and pluvial lake records (Ji et al., 2005a, 2005b; Yu et al., 2006; Herzschuh, 2006; Zhu et al., 2009; Mischke and Zhang, 2010; Leipe et al., 2014) in Oman, China and India (Fig. 9). We tentatively associate this possible climatic linkage recorded widely in multiple proxy records with glacial advances in the northwestern Himalaya and Tibet.

7.2.3. HH 6 (~8.2–7.4 ka)

HH 6 has a weighted mean age of 7.8 ± 0.2 ka with local glacial stages ranging from ~8.2 to 7.4 ka (Figs. 8B and 9; Table 4). This stage is recorded in three valleys in Muztag Ata with ΔELAs ranging between ~612 and 144 m (see Supplementary materials S9). Coeval glacier advances were also recorded in the semi-arid Zanskar (Sharma et al., 2016), the monsoonal southeastern and central

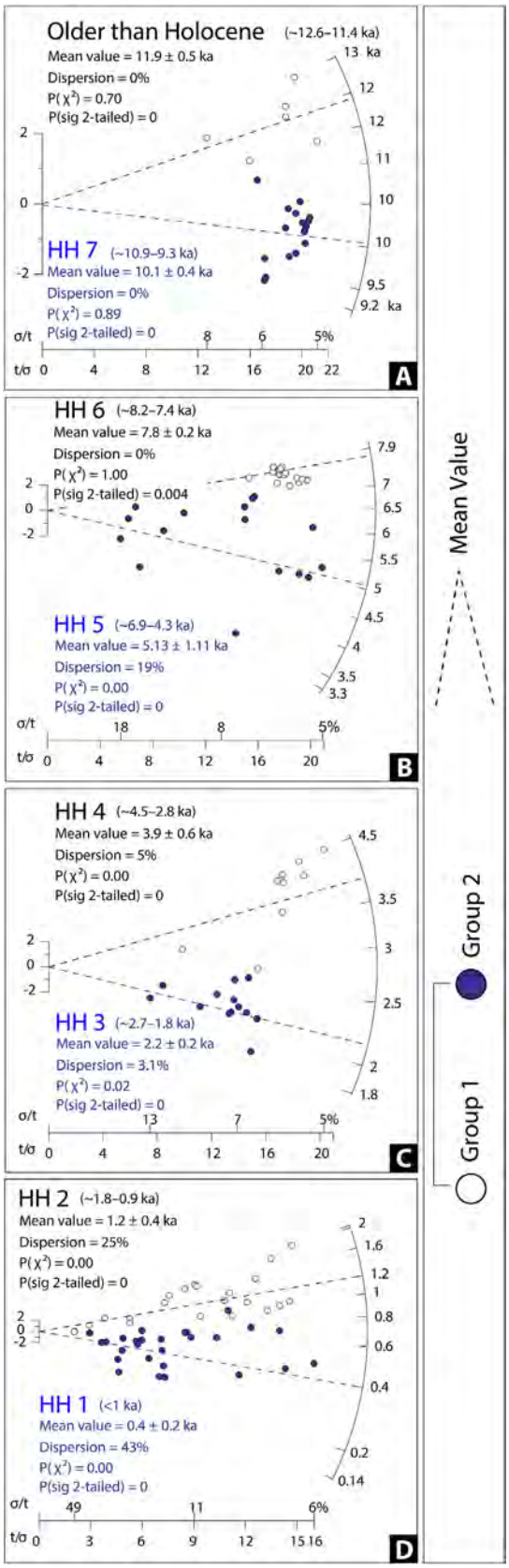

Fig. 8. Radial plots for outlier-free individual boulder ages comparing statistically significant two nearest age clusters, reported here as regional glacial stages, per selected timescale. We separately plotted two adjacent groups in each plot to demonstrate the statistical differences including their mean ages. Note: open and closed-blue circles represent two nearest but different age population in each plot. Regional glacial stages are arranged in descending chronological order from A through D. These results also show insignificant $P_{(sig\ 2\text{-}tailed)}$ distributions. Dashed lines represent the weighted mean of each population. Note that 1σ uncertainties for regional glacial stages are reported. (For interpretation of the references to color in this figure legend, the reader is referred to the Web version of this article.)

Himalaya (Bisht et al., 2015), and arid northern Tibet (MOHITS 1H at 8.1 ± 0.8 ka and MOHITS 1G at 7.7 ± 0.6 ka of Murari et al., 2014 and references therein), but the ΔELAs have not be determined for these regions. Abrupt temperature lowering with aridity during this time is also recorded extensively in several lake records from Tibet and has been linked to abrupt North Atlantic cooling between 8.5 and 8.2 ka (Ji et al., 2005a, 2005b; Kramer et al., 2010; Mischke and Zhang, 2010).

7.2.4. HH 5 (~6.9–4.3 ka)

HH 5 has a weighted mean of 5.1 ± 1.1 ka and is evident in four glaciated valleys (Figs. 8B and 9; Table 4). The ΔELAs in Lahul and Muztag Ata are comparable (~172–160 m), but relatively larger in the Central Karakoram (~622 ± 250 m; see Supplementary materials S9). Equivalent glacier advances are also reported in the more monsoonal central Himalaya and southeastern Tibet (MOHITS 1F at 5.4 ± 0.6 ka of Murari et al., 2014 and references therein). However, our local glacial stages are limited and highly scattered (19% dispersion) to decipher the role of climate during this regional stage. Recently, Srivastava et al. (2017) suggested a cold-dry period in the Himalaya at ~5.4–3.8 ka with high-frequency oscillation of short-term wet-warm periods. Catchment specific variable climatic responses are also reported in several lakes in Tibet during this time (see the review of Herzschuh, 2006; and Zhang and Mischke, 2009; Mischke et al., 2010). Whether this stage is associated with stronger Indian Summer monsoon (moisture) in the early phase (~6 ka in Fig. 9) or later with North Atlantic cooling (temperature) that is teleconnected via mid-latitude westerlies cannot be determined.

7.2.5. HH 4 (~4.5–2.8 ka)

HH 4 has a weighted mean age of 3.9 ± 0.6 ka; its local glacial stages range from ~4.5 to 2.8 ka (Figs. 8C and 9; Table 4). Dortch et al. (2013) also identified a glacial stage at 3.8 ± 0.6 ka (SWHTS 1C). A larger ΔELA is reconstructed in the Puga valley of Zanskar (~426 ± 58 m) in the south relative to Muztag Ata (~212–153 m; see Supplementary materials S9). The onset of a cold reversal during this time, associated with North Atlantic cooling (Mayewski et al., 2004; Solomina et al., 2015), is also recorded in glacial records in the central Himalaya (MOHITS 1E at 3.5 ± 0.4 ka in Murari et al., 2014 and references therein), peat records in the Garhwal Himalaya (Phadtare, 2000; Srivastava et al., 2017), the marine record in the Arabian Sea (von Rad et al., 1999), and several lake records in eastern (Mischke et al., 2010; Kramer et al., 2010; Mischke and Zhang, 2010), central (Herzschuh et al., 2006), and southwest Tibet (Gasse et al., 1996; Yanhong et al., 2006).

7.2.6. HH 3 (~2.7–1.8 ka)

HH 3 has a weighted mean age of 2.2 ± 0.2 ka with local glacial stages ranging from ~2.7 to 1.8 ka (Figs. 8C and 9; Table 4). The ΔELAs are generally very small, but larger in Muztag Ata (~131 ± 24 m) than in Ladakh and Zanskar (~64–56 m; see Supplementary materials S9). Coeval glacier advances are also reported from the monsoonal central Himalaya (MOHITS 1D at 2.3 ± 0.1 ka of Murari et al., 2014 and references therein), although overall cold and dry conditions have been proposed during ~3.0–1.4 ka in the Garhwal Himalaya (Srivastava et al., 2017; Fig. 9). Due to small number of local glacial stages (n = 3), we cannot resolve the potential climate forcing for these glacier advances.

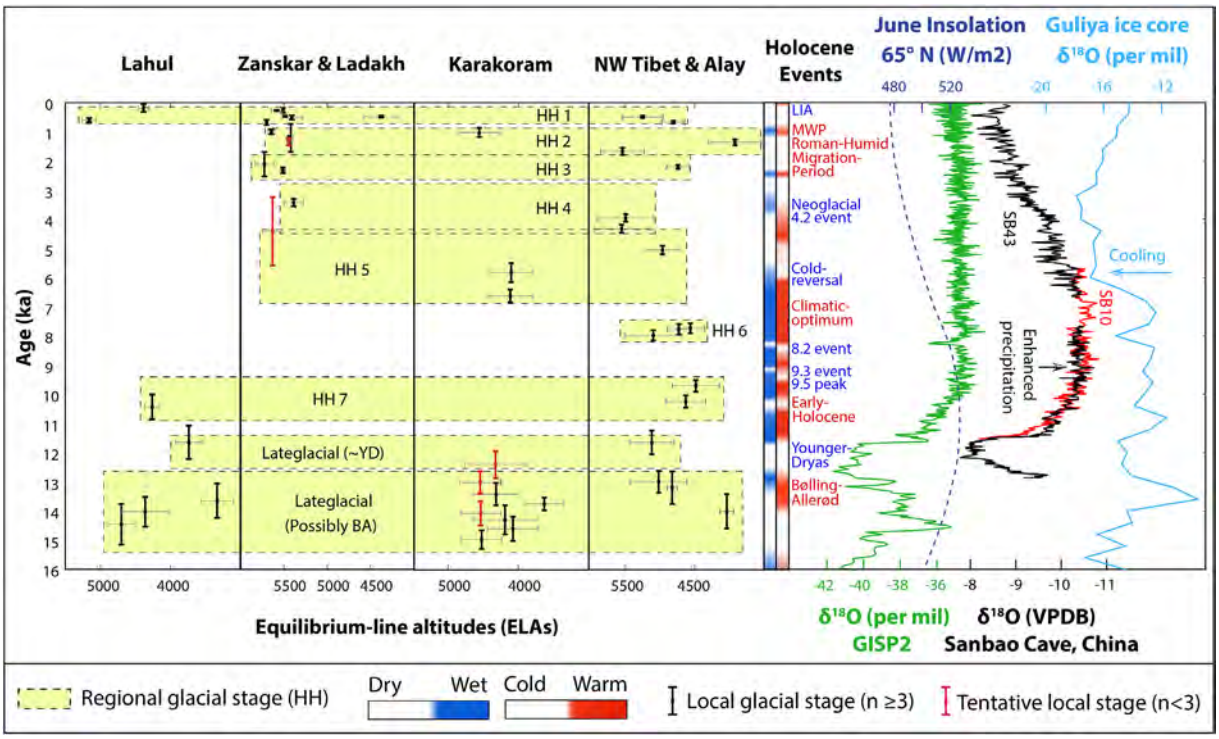

Fig. 9. Chronostratigraphies for Holocene regional glacial stages (HHs) in the northwestern end of the Himalaya and Tibet and coeval short-term climatic changes recorded in proxy records. HHs are arranged based on ELAs (x-axis) and organized according to (four) regions. A simplified summary of major Holocene climatic events is shown in the central part of the diagram and is reconstructed after Demske et al. (2009), Wünneman et al. (2010), Berkelhammer et al. (2012), Rawat et al. (2015a, 2015b), and Srivastava et al. (2017). Note that the color scheme does not correspond to magnitude of the change, but only the time range. Reconstructed orbital trend at 65°N latitude (after Berger, 1978), oxygen isotopes from Greenland ice cores—a proxy for temperature (Grootes and Stuiver, 1997.), from speleothems —a proxy for regional precipitation (Sanbao cave, China after Dong et al., 2010), and from Guliya ice cores—a proxy for regional temperature (Guliya ice core, Tibet after Thompson et al., 1997) are shown in the right for climatic interpretation. (For interpretation of the references to color in this figure legend, the reader is referred to the Web version of this article.)

7.2.7. HH 2 (~1.8–0.9 ka)

With local glacial stages ranging from ~1.8 to 0.9 ka and a weighted mean of 1.2 ± 0.4 ka, HH 2 was restricted in extent and is recorded in six glaciated valleys (Figs. 8D and 9; Table 4). The age dispersion for this HH is large (25%) indicating greater age scatter. ΔELAs are relatively large in Muztag Ata (~222–130 m) compared to the central Karakoram and Zanskar (~65–24 m; see Supplementary materials S9). The relative ΔELA differences between different types of glaciers in the north and south support the view that moisture supply increased in the northwestern Tibet occurred during this time. This stage correlates with MOHITS 1C at 1.5 ± 0.2 ka of Murari et al. (2014) in the humid eastern Himalaya. Whether stage 2 is associated with two cold events at ~1.7 and ~1.3 ka (Liu and Thompson, 1998; Mischke and Zhang, 2010; Yu et al., 2006) and/or intensified summer monsoon in the beginning of the Medieval Warm Period (Gupta et al., 2003; Dixit and Tandon, 2016; Srivastava et al., 2017) is impossible to resolve presently.

7.2.8. HH 1 (<1.0 ka)

Restricted local glacier advances are reconstructed during the last 1 ka in ten glaciated valleys, with HH stage 1 having a mean age of 0.4 ± 0.2 ka (Figs. 8D and 9; Table 4). Due to large age dispersion (43%) and overlapping ages, smaller sub-stages (e.g., MOHITS 1B at 0.7 ± 0.1 and MOHITS 1A at 0.4 ± 0.1 ka of Murari et al., 2014 in the monsoonal central Himalaya and southeastern Tibet) are speculative in our study areas. We suggest that this HH might corresponds to LIA cooling episodes associated with North Atlantic sea ice expansion and weakening of AMOC (Bond et al., 2001; Grove, 2004, 2008; Denton and Broecker, 2008) and is likely teleconnected by mid-latitude westerlies (Rowan, 2016). However, ΔELA were quite variable during this stage in our study areas. From south to north, ΔELAs range from ~167 to 57 m in Lahul, ~400–4 m in Zanskar, ~230 m in Ladakh, to ~68–63 m in Muztag Ata-Kongur Shan region (see Supplementary materials S9). Large scale regional variations in ΔELAs also suggest catchment specific climate response during this time and corroborate with the view that LIA was both cold and dry and cold and wet depending upon the catchment in the western Himalaya (Demske et al., 2009; Wünnemann et al., 2010; Rawat et al., 2015a, 2015b; Liang et al., 2015; Srivastava et al., 2017).

7.3. Holocene glacier advances and hemispheric climate linkages

We compare our Himalayan regional glacial chronostratigraphies to global glaciation datasets (see Mayewski et al., 2004; Grove, 2008; Davis et al., 2009; Luetscher et al., 2011; Schindelwig et al., 2012; Schimmelpfennig et al., 2012; Schimmelpfennig et al., 2014; Solomina et al., 2015, 2016 and references therein; Le Roy et al., 2015, 2017; Moran et al., 2015, 2016, 2017) and climate proxies derived from ice cores, lakes, and speleothems to help decipher the long-term climate forcing behind HHs (Fig. 9). These correlations are based on timing/chronozones, so they are accordingly speculative. We identify two regional late glacial and seven HHs (Fig. 9). The extent of glaciation varies significantly between each HH (see Supplementary material S9). Detailed studies of ΔELAs suggest relatively restricted glacial advances over time in each valley from Lateglacial/early Holocene through to the LIA (Fig. 10; see Supplementary material S1).

During the early Holocene (~10.9–9.3 ka) extensive glacial advances (ΔELA of ~425 ± 229 m), relative to their LIA advance, are recorded in the northwestern Himalaya and Tibet. Similar early

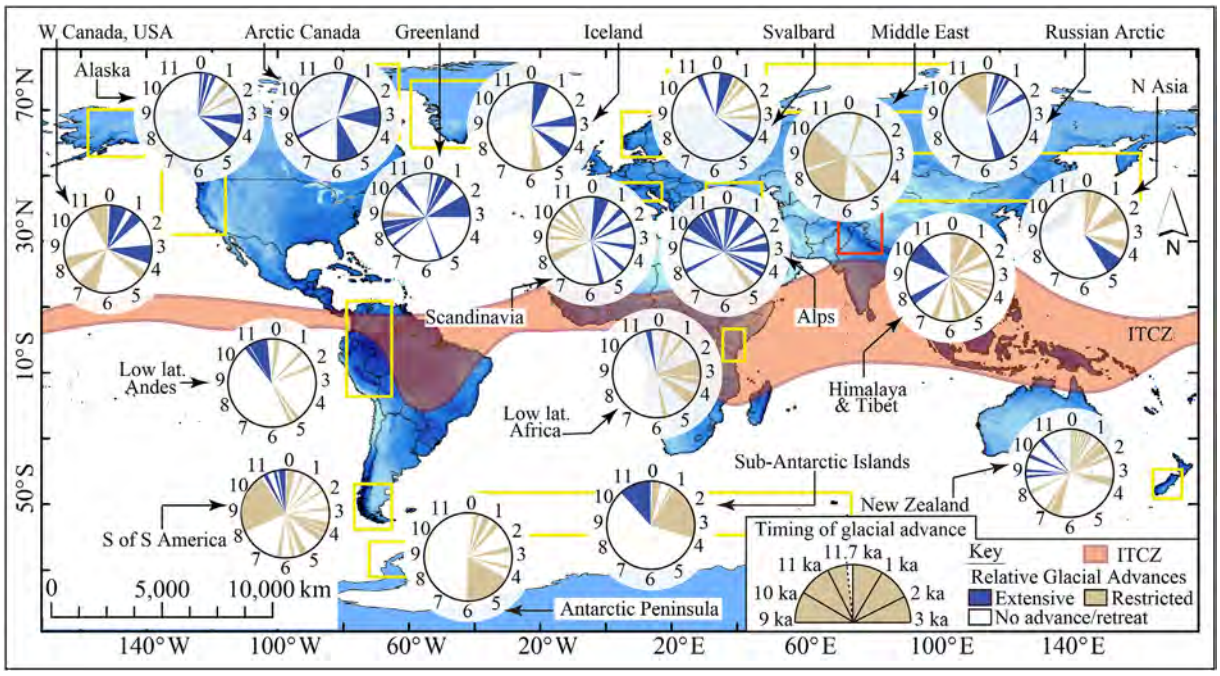

Fig. 10. Global seasonal distribution of ITCZ (see also Fig. 1A) and Holocene glacial chronostratigraphies compiled after Mayewski et al. (2004), Grove (2008), Davis et al. (2009), Luetscher et al. (2011), Schindelwig et al. (2012), Schimmelpfennig et al. (2012), Schimmelpfennig et al. (2014), Solomina et al. (2015, 2016 and references therein), Le Roy et al. (2015, 2017), and Moran et al. (2015, 2016, 2017). Clock diagrams showing the timing of glacier advances (in ka) with qualitative comparison of glacier extents during each chronozone. Here blue indicates *extensive advances* and pale brown *restricted glacier advances* relative to their LIA maximum. Our results for the northwestern Himalaya and Tibet are solely based on ^{10}Be ages with likely denote minimum age of glacial advance, whereas glacial records for other regions are based on variety of proxy climatic and glacial records, and hence partial obliteration of glacial records during subsequent extensive advances is likely minimum. To be consistent in our interpretation, only records of glacial advances (and not retreats) are shown here. Note also that here we present only Holocene glacial records (i.e., 11,700 years) and hence Younger Dryas records are not shown for focused discussion. (For interpretation of the references to color in this figure legend, the reader is referred to the Web version of this article.)

Holocene extensive glacier advances (~11–9.6 ka), larger than LIA maximum, are also recorded in European Alps (Schindelwig et al., 2012; Schimmelpfennig et al., 2012; Schimmelpfennig et al., 2014; Moran et al., 2015, 2016), Greenland (O'Hara et al., 2017), Arctic Canada (Young et al., 2012), Svalbard (van der Bilt et al., 2015), tropical Andes, Africa, and Southern Hemispheric extratropical regions (Fig. 10; Solomina et al., 2015, 2016 and references therein). Most of these early Holocene glacier advances in the high-latitudes of northern hemisphere are being attributed to cooling associated with the YD and short-term Preboreal Oscillation (PBO) in the Nordic Seas (Schindelwig et al., 2012; Moran et al., 2015, 2016), or regional fresh water input to north Atlantic sub-polar gyre (O'Hara et al., 2017). In contrast, early Holocene glacier advances in our study areas are most likely modulated by tropical/subtropical hydro-climatic changes and increased moisture supply and radiative cooling (see Rupper et al., 2009) corresponding to a northerly shifted Earth's thermal equator (ITCZ) and stronger monsoon (Wang et al., 2001, 2004; Lea et al., 2003; Jennerjahn et al., 2004; Dykoski et al., 2005; Severinghaus et al., 2009). Northward migration of large-scale atmospheric circulation systems associated with long-term orbital forcing likely favored high amplitude glacier advances in the northern hemisphere sub-tropics (e.g., our study area) and low-latitude tropical Andean and African glacier-systems (Levermann et al., 2009; Frierson and Hwang, 2011; Ceppi et al., 2013).

The subsequent early Holocene glacier advances, at ~8.2–7.4 ka, are also extensive in the northwestern Tibet compared to their LIA advance. Similar widespread high-amplitude glacial advances are also dated in the northern hemisphere extratropical glaciers (Solomina et al., 2015, 2016 and references therein; Cronauer et al., 2016) and attributed to changes in the North Atlantic Ocean condition (Alley et al., 1997; Davis et al., 2009; Eynaud et al., 2009). Possible teleconnection via mid-latitude westerlies are proposed for cooling during this time on the Tibetan Plateau (Thompson et al., 1997, 2003; Seong et al., 2009; Dortch et al., 2013).

Five HHs are recognized between the mid-Holocene and LIA (~6.9–0.2 ka) (Figs. 9 and 10). These glacier advances are comparatively more restricted in extent than early Holocene ones (ΔELA of ~141 ± 106 and ~124 ± 121 m in mid- and late-Holocene, respectively). Many extensive glacier advances, as large as the LIA maximum or larger (Luetscher et al., 2011; Moran et al., 2017; Le Roy et al., 2015, 2017), are also evident since at least ~4.3 ka in the northern hemisphere extratropical regions (Fig. 10). These glacier advances are attributed to reduced northern hemisphere insolation (Fig. 9) and corresponding north Atlantic sea-ice expansion, weakening of the Atlantic Meridional Overturning Circulation (Lund et al., 2006; Denton and Broecker, 2008; Chiang et al., 2014), and southerly shifted ITCZ and westerly wind belts (Haug et al., 2001; Sachs et al., 2009). The enhanced mid-latitude westerly winds likely teleconnected the cooling events in our study areas, but at subdued amplitude (Yancheva et al., 2007; Mölg et al., 2014; Srivastava et al., 2017). Our study, therefore, reinforces the concept of long-term orbitally influenced Holocene glaciation in the northwestern part of the Himalayan-Tibetan orogen and the possible amplification by large-scale migration of Earth's thermal equator and the associated hemispheric oceanic-atmospheric systems.

8. Conclusions

We define the long-term pattern of Holocene glacier advances at the northwestern end of the Himalayan-Tibetan orogen using 49

new and 187 recalculated published ^{10}Be moraine boulder ages from 32 glaciated valleys. Despite the large dispersion of individual ^{10}Be boulder ages on young moraines, our results suggest that in our four study areas, five Holocene glacial stages are locally recorded, including three synchronous advances. These date to ~10.4, ~6.1–3.3, ~2.1–0.9, ~0.7–0.4, and ~0.3–0.2 ka.

An extensive (>10 km) glacier advance and larger ΔELA (~182 ± 57 m) occurred in the early Holocene at ~10.4 ka in the more humid Hamtah study area in the Lahul Himalaya. Relative to early Holocene, middle and late Holocene glacier advances in our study areas were progressively restricted with ΔELAs ranging from ~160 to ~4 m. Glaciers advanced at ~0.2 ka in the Hamtah valley, at ~6.1–3.3 and ~2.1 ka in the Gomuche Kangri and at ~1.0 and ~0.7 ka in the Mentok Kangri valleys of Karzok, at ~0.5 and ~0.3 ka in the Lato study area and at ~2.1–0.9 ka in the Stok valley during the Holocene.

Seven HHs were determined by compiling 32 local glacial chronologies (new and published ages) for the northwestern end of the Himalayan-Tibetan orogen. These date to ~10.9–9.3, ~8.2–7.4, ~6.9–4.3, ~4.5–2.8, ~2.7–1.8, ~1.8–0.9, and <1 ka. These regional glacier advances are highly variable in each valley during different stages, but in general are relatively extensive for the early Holocene with mean ΔELAs of ~425 ± 229 m, compared to middle Holocene (mean ΔELA of ~141 ± 106 m), and late Holocene (mean ΔELA of ~124 ± 121 m). The spatial distribution of ΔELAs during different HHs indicate a complex interplay of topography, hypsometry, and moisture and temperature associated with the prevailing summer monsoon and mid-latitude winter westerlies. Based on the amplitude of Holocene glacier advances in the northwestern Himalaya and Tibet, we argue that they are analogous to glacier advances in the low latitudinal Andes, Africa, Peruvian Andes, and some extratropical regions in the Northern Hemisphere, i.e., progressively restricted from early to late Holocene. Nevertheless, the timing of majority of HHs during mid- and late Holocene indicates close correspondence with the North Atlantic cooling that is likely teleconnected via mid-latitude westerlies, especially during ~8 ka and after ~5 ka. In contrast, early Holocene glacier advances are driven by a northerly shifted ITCZ and enhanced monsoon activities in the region. We interpret this long-term pattern of Holocene glacier advances to be likely influenced by orbital forcing and amplified by large-scale migration of Earth's thermal equator and the associated hemispheric oceanic-atmospheric systems. Future studies should verify these findings with high-frequency Holocene glacier advances across the entire orogen.

Acknowledgments

We like to thank anonymous reviewers, the editor, Craig Dietsch, Dylan Ward, Thomas Lowell, and Richard Beck for constructive suggestions on this project. SS, LAO and ENO thank the Department of Geology at the University of Cincinnati for fieldwork support. SS acknowledges support from the Geological Society of America for Graduate Student Research Grant and the Graduate Student Governance Association, University of Cincinnati for Research Fellowship to conduct fieldwork. Sincere thanks to Tsewang Dorjee and his team for logistical support and Charles de Luzan for helping with MATLAB scripts. MWC acknowledges support from NSF (EAR-1560658).

Appendix A. Supplementary data

Supplementary data related to this article can be found at https://doi.org/10.1016/j.quascirev.2018.03.009.

References

Abramowski, U., Bergau, A., Seebach, D., Zech, R., Glaser, B., Sosin, P., Kubik, P.W., Zech, W., 2006. Pleistocene glaciations of Central Asia: results from ^{10}Be surface exposure ages of erratic boulders from the Pamir (Tajikistan), and the Alay–Turkestan range (Kyrgyzstan). Quat. Sci. Rev. 25, 1080–1096.
Alley, R.B., Cuffey, K.M., Evenson, E.B., Strasser, J.C., Lawson, D.E., Larsonh, G.J., 1997. How glaciers entrain and transport basal sediment: physical constraints. Quat. Sci. Rev. 16, 1017–1038.
Anderson, R.S., Dühnforth, M., Colgan, W., Anderson, L., 2012. Far-flung moraines: exploring the feedback of glacial erosion on the evolution of glacier length. Geomorphology 179, 269–285.
Andrews, J.T., 1975. Glacial Systems. An Approach to G/aciers and Their Enrironments. Duxbury Press, North Scituate, p. 191.
Applegate, P.J., Urban, N.M., Keller, K., Lowell, T.V., Laabs, B.J.C., Kelly, M., a, Alley, R.B., 2012. Improved moraine age interpretations through explicit matching of geomorphic process models to cosmogenic nuclide measurements from single landforms. Quat. Res. (Duluth) 77, 293–304.
Applegate, P.J., Urban, N.M., Laabs, B.J.C., Keller, K., Alley, R.B., 2010. Modeling the statistical distributions of cosmogenic exposure dates from moraines. Geosci. Model Dev. (GMD) 3, 293–307.
Azam, M.F., Wagnon, P., Vincent, C., Ramanathan, A., Favier, V., Mandal, A., Pottakkal, J.G., 2014. Processes governing the mass balance of Chhota Shigri Glacier (western Himalaya, India) assessed by point-scale surface energy balance measurements. Cryosphere 8, 2195–2217.
Balco, G., Stone, J.O., Lifton, N., a, Dunai, T.J., 2008. A complete and easily accessible means of calculating surface exposure ages or erosion rates from ^{10}Be and ^{26}Al measurements. Quat. Geochronol. 3, 174–195.
Ballantyne, C.K., McCarroll, D., Stone, J.O., 2007. The Donegal ice dome, northwest Ireland: dimensions and chronology. J. Quat. Sci. 22, 773–783.
Barr, I.D., Clark, C.D., 2012. Late Quaternary glaciations in Far NE Russia; combining moraines, topography and chronology to assess regional and global glaciation synchrony. Quat. Sci. Rev. 53, 72–87.
Barr, I.D., Lovell, H., 2014. A review of topographic controls on moraine distribution. Geomorphology 226, 44–64.
Barrows, T.T., 2007. Absence of cooling in New Zealand. Geology 86, 86–89.
Benn, D.I., Ballantyne, C.K., 2005. Palaeoclimatic reconstruction from loch lomond readvance glaciers in the west drumochter hills. Scotland. J. Quat. Sci. 20, 577–592.
Benn, D.I., Lehmkuhl, F., 2000. Mass balance and equilibrium-line altitudes of glaciers in high-mountain environments. Quat. Int. 65–66, 15–29.
Benn, D.I., Owen, L.A., 1998. The role of the Indian summer monsoon and the mid-latitude westerlies in Himalayan glaciation: review and speculative discussion. J. Geol. Soc. London 155, 353–363.
Benn, D.I., Owen, L.A., 2002. Himalayan glacial sedimentary environments: a framework for reconstructing and dating former glacial extents in high mountain regions. Quat. Int. 97–98, 3–26.
Benn, D.I., Owen, L.A., Osmaston, H.A., Seltzer, G.O., Porter, S.C., Mark, B., 2005. Reconstruction of equilibrium-line altitudes for tropical and sub-tropical glaciers, 139, 8–21.
Berger, A., 1978. Long-term variations of caloric insolation resulting from the earth's orbital elements. Quat. Res. (Duluth) 9, 139–167.
Berkelhammer, M., Sinha, A., Stott, L., Cheng, H., Pausata, F.S.R., Yoshimura, K., 2012. An abrupt shift in the indian monsoon 4, 000 years ago an abrupt shift in the indian monsoon 4000 Years ago. Climates, Landsc. Civiliz 75–88.
Bisht, P., Ali, S.N., Shukla, A.D., Negi, S., Sundriyal, Y.P., Yadava, M.G., Juyal, N., 2015. Chronology of late Quaternary glaciation and landform evolution in the upper Dhauliganga valley, (Trans Himalaya), Uttarakhand, India. Quat. Sci. Rev. 129, 147–162.
Bond, G., Kromer, B., Beer, J., Muscheler, R., Evans, M.N., Showers, W., Hoffmann, S., Lotti-Bond, R., Hajdas, I., Bonani, G., 2001. Persistent solar influence on north Atlantic climate during the Holocene. Science 294, 2130–2136.
Bookhagen, B., Burbank, D.W., 2006. Topography, relief, and TRMM-derived rainfall variations along the Himalaya. Geophys. Res. Lett. 33, 1–5. L08405.
Borchers, B., Marrero, S., Balco, G., Caffee, M., Goehring, B., Lifton, N., Nishiizumi, K., Phillips, F., Schaefer, J., Stone, J., 2016. Geological calibration of spallation production rates in the CRONUS-Earth project. Quat. Geochronol. 31, 188–198.
Brookfield, M.E., Andrews-Speed, C.P., 1984. Sedimentology, petrography and tectonic significance of the shelf, flysch and molasse clastic deposits across the Indus Suture Zone, Ladakh, NW India. Sediment. Geol. 40, 249–286.
Burbank, D.W., Cheng, K.J., 1991. Relative dating of quaternary moraines, rongbuk valley, mount everest, Tibet: implications for an ice sheet on the Tibetan plateau. Quat. Res. (Duluth) 36, 1–18.
Burbank, D.W., Fort, M.B., 1985. Bedrock control on glacial limits: examples from the ladakh and zanskar ranges, north-western Himalaya, India. J. Glaciol. 31, 143–149.
Ceppi, P., Hwang, Y.T., Liu, X., Frierson, D.M.W., Hartmann, D.L., 2013. The relationship between the ITCZ and the Southern Hemispheric eddy-driven jet. J. Geophys. Res. Atmos. 118, 5136–5146.
Chiang, J.C.H., Friedman, A.R., 2012. Extratropical cooling, interhemispheric thermal gradients, and tropical climate change. Annu. Rev. Earth Planet Sci. 40, 383–412.
Chiang, J.C.H., Lee, S.Y., Putnam, A.E., Wang, X., 2014. South Pacific Split Jet, ITCZ shifts, and atmospheric North-South linkages during abrupt climate changes of

the last glacial period. Earth Planet Sci. Lett. 406, 233–246.
Corbett, L.B., Bierman, P.R., Rood, D.H., 2016. An approach for optimizing in situ cosmogenic ^{10}Be sample preparation. Quat. Geochronol. 33, 24–34.
Cronauer, S.L., Briner, J.P., Kelley, S.E., Zimmerman, S.R.H., Morlighem, M., 2016. 10Be dating reveals early-middle Holocene age of the Drygalski Moraines in central West Greenland. Quat. Sci. Rev. 147, 59–68.
Dahl, S.O., Nesje, A., 1992. Paleoclimatic implications based on equilibrium-line altitude depressions of reconstructed Younger Dryas and Holocene cirque glaciers in inner Nordfjord, western Norway. Palaeogeogr. Palaeoclimatol. Palaeoecol. 94, 87–97.
Davis, P.T., Menounos, B., Osborn, G., 2009. Holocene and latest Pleistocene alpine glacier fluctuations: a global perspective. Quat. Sci. Rev. 28, 2021–2033.
Demske, D., Tarasov, P.E., Wünnemann, B., Riedel, F., 2009. Late glacial and Holocene vegetation, Indian monsoon and westerly circulation in the Trans-Himalaya recorded in the lacustrine pollen sequence from Tso Kar. Palaeogeogr. Palaeoclimatol. Palaeoecol. 279, 172–185.
Denton, G.H., Broecker, W.S., 2008. Wobbly ocean conveyor circulation during the Holocene? Quat. Sci. Rev. 27, 1939–1950.
Desilets, D., Zreda, M., Prabu, T., 2006. Extended scaling factors for in situ cosmogenic nuclides: new measurements at low latitude. Earth Planet Sci. Lett. 246, 265–276.
Dietsch, C., Dortch, J., Reynhout, S., Owen, L., Caffee, M., 2015. Very slow erosion and topographic evolution of the Southern Ladakh Range, India. Earth Surf. Process. Landforms 40 (3), 389–402.
Dixit, Y., Tandon, S.K., 2016. Hydroclimatic variability on the Indian subcontinent in the past millennium: review and assessment. Earth Sci. Rev. 161, 1–15.
Dong, J., Wang, Y., Cheng, H., Hardt, B., Edwards, R.L., Kong, X., Wu, J., Chen, S., Liu, D., Jiang, X., Zhao, K., 2010. A high-resolution stalagmite record of the Holocene East Asian monsoon from Mt Shennongjia, central China. Holocene 20, 257–264.
Dortch, J., Owen, L., Schoenbohm, L., Caffee, M., 2011. Asymmetrical erosion and morphological development of the central Ladakh Range, northern India. Geomorphology 135, 167–180.
Dortch, J.M., Owen, L.A., Caffee, M.W., 2013. Timing and climatic drivers for glaciation across semi-arid western Himalayan–Tibetan orogen. Quat. Sci. Rev. 78, 188–208.
Dunai, T.J., 2001. Influence of secular variation of the geomagnetic field on production rates of in situ produced cosmogenic nuclides. Earth Planet Sci. Lett. 193, 197–212.
Dunai, T.J., 2010. Cosmogenic Nuclides: Principles, Concepts and Applications in the Earth Surface Sciences. Cambridge Univ. Press, Cambridge.
Dyke, A.S., Savelle, J.M., 2000. Major end moraines of younger Dryas age on wollaston peninsula, victoria island, canadian arctic: implications for paleoclimate and for formation of hummocky moraine. Can. J. Earth Sci. 37, 601–619.
Dykoski, C.A., Edwards, R.L., Cheng, H., Yuan, D., Cai, Y., Zhang, M., Lin, Y., Qing, J., An, Z., Revenaugh, J., 2005. A high-resolution, absolute-dated Holocene and deglacial Asian monsoon record from Dongge Cave, China. Earth Planet Sci. Lett. 233, 71–86.
Epard, J.L., Steck, A., 2008. Structural development of the Tso morari ultra-high pressure nappe of the ladakh Himalaya. Tectonophysics 451, 242–264.
Eugster, P., Scherler, D., Thiede, R.C., Codilean, A.T., Strecker, M.R., 2016. Rapid last glacial maximum deglaciation in the Indian Himalaya coeval with mid-latitude glaciers: new insights from ^{10}Be-dating of ice-polished bedrock surfaces in the Chandra Valley, NW Himalaya. Geophys. Res. Lett. 43, 1589–1597.
Eynaud, F., de Abreu, L., Voelker, A., Schönfeld, J., Salgueiro, E., Turon, J.L., Penaud, A., Toucanne, S., Naughton, F., Sánchez Goñi, M.F., Malaizé, B., Cacho, I., 2009. Position of the Polar Front along the western Iberian margin during key cold episodes of the last 45 ka. G-cubed 10, 1–21.
Fleitmann, D., Burns, S.J., Mangini, A., Mudelsee, M., Kramers, J., Villa, I., Neff, U., Al-Subbary, A.A., Buettner, A., Hippler, D., Matter, A., 2007. Holocene ITCZ and Indian monsoon dynamics recorded in stalagmites from Oman and Yemen (Socotra). Quat. Sci. Rev. 26, 170–188.
Fleitmann, D., Burns, S.J., Mudelsee, M., Neff, U., Kramers, J., Mangini, A., Matter, A., 2003. Holocene forcing of the indian monsoon recorded in a stalagmite from southern Oman. Science (Wash. D C) 300, 1737–1739.
Fort, M., 1995. The Himalayan glaciation: myth and reality. Journal of Nepal Geological Society Special Issue 11, 257–272.
Frierson, D.M.W., Hwang, Y.T., 2011. Extratropical influence on ITCZ shifts in slab ocean simulations of global warming. J. Clim. 25, 720–733.
Fuchs, Gerhard, Linner, Manfred, 1996. On the Geology of the Suture Zone and Tso Morari Dome in Eastern Ladakh (Himalaya). Jb. Geol. Bundesanstalt, Wien 139, pp. 191–207.
Galbraith, R.F., 1990. The radial plot: graphical assessment of the spread in ages. Nucl. Tracks Radiat. Meas. 17, 207–214.
Galbraith, R.F., 2010. On plotting OSL equivalent doses. Anc. TL 28, 1–10.
Galbraith, R.F., Roberts, R.G., 2012. Statistical aspects of equivalent dose and error calculation and display in OSL dating: an overview and some recommendations. Quat. Geochronol. 11, 1–27.
Gasse, F., Fontes, J.C., Campo, E., Van, Wei, K., 1996. Holocene environmental changes in bangong Co basin (western Tibet). Part 4: discussion and conclusions, 120, 79–92.
Gibbons, A.B., Megeath, J.D., Pierce, K.L., 1984. Probability of moraine survival in a succession of glacial advances. Geology 12, 327–330.
Gillespie, A., Rupper, S., Roe, G., 2003. Climatic interpretation from mountain glaciations in Central Asia. In: XVI INQUA Congress Programs with Abstracts, p. 170. DRI, Reno, Nv.
Gosse, J.C., 2005. The contributions of cosmogenic nuclides to unraveling alpine paleo-glacier histories. In: Huber, U.M., Bugmann, H.K.M., Reasoner, M.A. (Eds.), Global Change and Mountain Regions. An Overview of Current Knowledge. Advances in Global Change Research, vol. 23. Springer, Dordrecht, pp. 39–50.
Gosse, J.C., Phillips, F.M., 2001. Terrestrial in situ cosmogenic nuclides: theory and application. Quat. Sci. Rev. 20, 1475–1560.
Grootes, P.M., Stuiver, M., 1997. Oxygen 18/16 variability in Greenland snow and ice with 10^{-3}- to 10^{5}-year time resolution. J. Geophys. Res. 102, 26455–26470.
Grove, A.T., 2008. A brief consideration of climate forcing factors in view of the Holocene glacier record. Global Planet. Change 60, 141–147.
Grove, J.M., 2004. Little Ice Ages Ancient and Modern, second ed., 2 vols. Routledge, London.
Gupta, A.K., Anderson, D.M., Overpeck, J.T., 2003. Abrupt changes in the asian southwest monsoon during the Holocene and their links to the north Atlantic Ocean. Nature 421, 354–357.
Haug, G.H., Hughen, K.A., Sigman, D.M., Peterson, L.C., Ro, U., 2001. Southward migration of the intertropical convergence zone through the Holocene. Science 293, 1304–1308.
Hedrick, K.A., Seong, Y.B., Owen, L.A., Caffee, M.W., Dietsch, C., 2011. Towards defining the transition in style and timing of Quaternary glaciation between the monsoon-influenced Greater Himalaya and the semi-arid Transhimalaya of Northern. India. Quat. Int 236, 21–33.
Heimsath, A.M., McGlynn, R., 2008. Quantifying periglacial erosion in the Nepal high Himalaya. Geomorphology 97, 5–23.
Herzschuh, U., 2006. Palaeo-moisture evolution in monsoonal Central Asia during the last 50,000 years. Quat. Sci. Rev. 25, 163–178.
Herzschuh, U., Winter, K., Wünnemann, B., Li, S., 2006. A general cooling trend on the central Tibetan Plateau throughout the Holocene recorded by the Lake Zigetang pollen spectra. Quat. Int. 154–155, 113–121.
Heyman, J., 2014. Paleoglaciation of the Tibetan plateau and surrounding mountains based on exposure ages and ELA depression estimates. Quat. Sci. Rev. 91, 30–41.
Hobley, D., Sinclair, H., Cowie, P., 2010. Processes, rates, and timescales of fluvial response in an ancient postglacial landscape of the northwest Indian Himalaya. Geol. Soc. Am. Bull. 122, 1569–1584.
Honegger, K., Dietrich, V., Frank, W., Gansser, A., Thöni, M., Trommsdorff, V., 1982. Magmatism and metamorphism in the Ladakh Himalayas (the Indus–Tsangpo suture zone). Earth Planet Sci. Lett. 60, 253–292.
Hu, C., Henderson, G.M., Huang, J., Xie, S., Sun, Y., Johnson, K.R., 2008. Quantification of Holocene Asian monsoon rainfall from spatially separated cave records. Earth Planet Sci. Lett. 266, 221–232.
Hughes, P.D., 2010. Geomorphology and Quaternary stratigraphy: the roles of morpho-, litho-, and allostratigraphy. Geomorphology 123, 189–199.
Hughes, P.D., Gibbard, P.L., Woodward, J., 2005. Quaternary glacial records in mountain regions: a formal stratigraphical approach. Episodes 28, 85–92.
Ivy-Ochs, S., Kerschner, H., Schlüchter, C., 2007. Cosmogenic nuclides and the dating of Lateglacial and Early Holocene glacier variations: the Alpine perspective. Quat. Int. 164–165, 53–63.
Jennerjahn, T.C., Ittekkot, V., Arz, H.W., Behling, H., Pätzold, J., Wefer, G., 2004. Asynchronous terrestrial and marine signals of climate change during heinrich events asynchronous terrestrial and marine signals of climate change during heinrich events. Science (Wash. D C) 306.
Ji, J., Shen, J., Balsam, W., Chen, J., Liu, L., Liu, X., 2005a. Asian monsoon oscillations in the northeastern Qinghai-Tibet Plateau since the late glacial as interpreted from visible reflectance of Qinghai Lake sediments. Earth Planet Sci. Lett. 233, 61–70.
Ji, S., Xingqi, L., Sumin, W., Matsumoto, R., 2005b. Palaeoclimatic changes in the Qinghai Lake area during the last 18,000 years. Quat. Int. 136, 131–140.
Kaplan, M.R., Hein, A.S., Hubbard, A., Lax, S.M., 2009. Can glacial erosion limit the extent of glaciation? Geomorphology 103, 172–179.
Kaplan, M.R., Schaefer, J.M., Denton, G.H., Doughty, A.M., Barrell, D.J.A., Chinn, T.J.H., Putnam, A.E., Andersen, B.G., Mackintosh, A., Finkel, R.C., Schwartz, R., Anderson, B., 2013. The anatomy of long-term warming since 15 ka in New Zealand based on net glacier snowline rise. Geology 41, 887–890.
Kaser, G., Osmaston, H., 2002. Tropical Glaciers. Cambridge University Press, Cambridge, p. 207.
Kirkbride, M.P., Brazier, V., 1998. A critical evaluation of the use of glacier chronologies in climate reconstruction, with reference to New Zealand. Quat. Proc. 6, 55–64.
Kirkbride, M.P., Winkler, S., 2012. Correlation of Late Quaternary moraines: impact of climate variability, glacier response, and chronological resolution. Quat. Sci. Rev. 46, 1–29.
Kohl, C.P., Nishiizumi, K., 1992. Chemical isolation of quartz for measurement of in-situ produced cosmogenic nuclides. Geochem. Cosmochim. Acta 56, 3583–3587.
Kramer, A., Herzschuh, U., Mischke, S., Zhang, C., 2010. Holocene treeline shifts and monsoon variability in the Hengduan Mountains (southeastern Tibetan Plateau), implications from palynological investigations. Palaeogeogr. Palaeoclimatol. Palaeoecol. 286, 23–41.
Kulkarni, A.V., 1992. Mass balance of Hilnalayan glaciers using AAR and ELA Methods. J. Glaciol. 38, 101–104.
Kumar, G., Joshi, A., Mathur, V.K., 1987. Redlichid trilobites from the tal formation. Lesser Himalaya. India. Curr. Sci. 56, 659–663.
Lal, D., 1991. Cosmic ray labeling of erosion surfaces: in situ nuclide production rates and erosion models. Earth Planet Sci. Lett. 104, 424–439.

Lavé, J., Avouac, J.P., 2001. Fluvial incision and tectonic uplift across the Himalayas of central Nepal. J. Geophys. Res. 106, 26561–26591.
Le Roy, M., Deline, P., Carcaillet, J., Schimmelpfennig, I., Ermini, M., Team, A.S.T.E.R., 2017. 10Be exposure dating of the timing of Neoglacial glacier advances in the Ecrins-Pelvoux massif, southern French Alps. Quat. Sci. Rev. 178, 118–138.
Le Roy, M., Nicolussi, K., Deline, P., Astrade, L., Edouard, J.L., Miramont, C., Arnaud, F., 2015. Calendar-dated glacier variations in the western European Alps during the Neoglacial: the Mer de Glace record, Mont Blanc massif. Quat. Sci. Rev. 108, 1–22.
Lea, D.W., Pak, D.K., Peterson, L.C., Hughen, K.A., 2003. Synchroneity of tropical and high-latitude atlantic temperatures over the last glacial termination. Science 301, 1361–1364.
Lee, S.Y., Seong, Y.B., Owen, L., a., Murari, M.K., Lim, H.S., Yoon, H. Il, Yoo, K.C., 2014. Late Quaternary glaciation in the Nun-Kun massif, northwestern India. Boreas 43, 67–89.
Leipe, C., Demske, D., Tarasov, P.E., 2014. A Holocene pollen record from the northwestern Himalayan lake Tso Moriri: implications for palaeoclimatic and archaeological research. Quat. Int. 348, 93–112.
Levermann, A., Schewe, J., Petoukhov, V., Held, H., 2009. Basic mechanism for abrupt monsoon transitions. Proc. Natl. Acad. Sci. Unit. States Am. 106, 20572–20577.
Liang, F., Brook, G.A., Kotlia, B.S., Railsback, L.B., Hardt, B., Cheng, H., Edwards, R.L., Kandasamy, S., 2015. Panigarh cave stalagmite evidence of climate change in the Indian Central Himalaya since AD 1256: monsoon breaks and winter southern jet depressions. Quat. Sci. Rev. 124, 145–161.
Lifton, N., 2016. Implications of two Holocene time-dependent geomagnetic models for cosmogenic nuclide production rate scaling. Earth Planet Sci. Lett. 433, 257–268.
Lifton, N., Sato, T., Dunai, T.J., 2014. Scaling in situ cosmogenic nuclide production rates using analytical approximations to atmospheric cosmic-ray fluxes. Earth Planet Sci. Lett. 386, 149–160.
Lifton, N.A., Bieber, J.W., Clem, J.M., Duldig, M.L., Evenson, P., Humble, J.E., Pyle, R., 2005. Addressing solar modulation and long-term uncertainties in scaling secondary cosmic rays for in situ cosmogenic nuclide applications. Earth Planet Sci. Lett. 239, 140–161.
Lifton, N.A., Smart, D.F., Shea, M.A., 2008. Scaling time-integrated in situ cosmogenic nuclide production rates using a continuous geomagnetic model. Earth Planet Sci. Lett. 268, 190–201.
Liu, K., Thompson, L.G., 1998. A pollen record of Holocene climatic changes from the Dunde ice cap, Qinghai-Tibetan Plateau. Geology 1986, 135–138.
Luetscher, M., Hoffmann, D.L., Frisia, S., Spötl, C., 2011. Holocene glacier history from alpine speleothems, Milchbach cave. Switzerland. Earth Planet. Sci. Lett. 302, 95–106.
Lund, D.C., Lynch-stieglitz, J., Curry, W.B., 2006. Gulf Stream density structure and transport during the past millennium. Nature 444, 601–604.
Macgregor, K.R., Anderson, R.S., Program, E.D.W.G., 2000. Numerical simulations of glacial-valley longitudinal profile evolution. Geology 28, 1031–1034.
Marrero, S., Phillips, F., Borchers, B., Lifton, N., 2016. Cosmogenic nuclide systematics and the CRONUScalc program. Quat. Geochronol 31, 1–72.
Martin, L.C.P., Blard, P.H., Balco, G., Lavé, J., Delunel, R., Lifton, N., Laurent, V., 2016. The CREp program and the ICE-D production rate calibration database: a fully parameterizable and updated online tool to compute cosmic-ray exposure ages. Quat. Geochronol 38, 25–49.
Mayewski, P., a, Rohling, E., Curtstager, J., Karlén, W., Maasch, K., Davidmeeker, L., Meyerson, E., Gasse, F., Vankreveld, S., Holmgren, K., 2004. Holocene climate variability. Quat. Res. (Duluth) 62, 243–255.
Mischke, S., Zhang, C., 2010. Holocene cold events on the Tibetan Plateau. Global Planet. Change 72, 155–163.
Mischke, S., Zhang, C., Börner, A., Herzschuh, U., 2010. Lateglacial and Holocene variation in aeolian sediment flux over the northeastern Tibetan Plateau recorded by laminated sediments of a saline meromictic lake. J. Quat. Sci. 25, 162–177.
Mölg, T., Maussion, F., Scherer, D., 2014. Mid-latitude westerlies as a driver of glacier variability in monsoonal High Asia. Nat. Clim. Change 4, 68–73.
Moran, A.P., Ivy Ochs, S., Christl, M., Kerschner, H., 2017. Exposure dating of a pronounced glacier advance at the onset of the late-Holocene in the central Tyrolean Alps. Holocene 27, 1350–1358.
Moran, A.P., Ivy-Ochs, S., Schuh, M., Christl, M., Kerschner, H., 2016. Evidence of central Alpine glacier advances during the Younger Dryas–early Holocene transition period. Boreas 45, 398–410.
Moran, A.P., Kerschner, H., Ochs, S.I., 2015. Redating the moraines in the kromer valley (silvretta mountains) – new evidence for an early Holocene glacier advance. Holocene 26, 655–664.
Murari, M.K., Owen, L.A., Dortch, J.M., Caffee, M.W., Dietsch, C., Fuchs, M., Haneberg, W.C., Sharma, M.C., Townsend-Small, A., 2014. Timing and climatic drivers for glaciation across monsoon-influenced regions of the Himalayan–Tibetan orogen. Quat. Sci. Rev. 88, 159–182.
New, M., Lister, D., Hulme, M., Makin, I., 2002. A high-resolution data set of surface climate over global land areas. Clim. Res. 21, 1–25.
Nishiizumi, K., Finkel, R.C., Caffee, M.W., Southon, J.R., Kohl, C.P., Arnold, J.R., Olinger, C.T., Poths, J., Klein, J., 1994. Cosmogenic Production of 10Be and 26Al on the Surface of the Earth and Underground. In: Eighth International Conference on Geochronology, Cosmochronology and Isotope Geochemistry. U.S. Geol. Surv. Circular 1107, Berkeley, California, p. 234.
Nishiizumi, K., Imamura, M., Caffee, M.W., Southon, J.R., Finkel, R.C., Mcaninch, J., 2007. Be AMS standards. Nucl. Instrum. Meth. Phys. Res. B 258, 403–413.
O'Hara, S.L., Briner, J.P., Kelley, S.E., 2017. A10Be chronology of early Holocene local glacier moraines in central West Greenland. Boreas 46, 655–666.
Oerlemans, J., 2005. Extracting a climate signal from 169 glacier records. Science 308, 675–677.
Oerlemans, J., 2010. The Microclimate of Valley Glaciers. Igitur, Utrecht Publishing & Archiving Services. Universiteitsbibliotheek Utrecht, The Netherlands, p. 138.
Orr, E.N., Owen, L.A., Murari, M.K., Saha, S., Caffee, M.W., 2017. Geomorphology the timing and extent of Quaternary glaciation of Stok, northern Zanskar. Geomorphology 284, 142–155.
Orr, E.N., Owen, L.A., Saha, S., Caffee, M.W., Muraria, M.K., 2018. Quaternary Glaciation of the Lato Massif, Zanskar Range of the NW Himalaya. Quat. Sci Rev. 183, 140–156.
Osmaston, H., 2005. Estimates of glacier equilibrium line altitudes by the Area x altitude, the Area x altitude balance ratio and the Area x altitude balance index methods and their validation. Quat. Int. 138–139, 22–31.
Owen, L.A., Finkel, R.C., Caffee, M.W., 2002. A note on the extent of glaciation throughout the Himalaya during the global Last Glacial Maximum. Quat. Sci. Rev. 21, 147–157.
Owen, L.A., Benn, D.I., 2005. Equilibrium-line altitudes of the last glacial maximum for the Himalaya and Tibet: an assessment and evaluation of results. Quat. Int. 138–139, 55–78.
Owen, L.A., Derbyshire, E., Richardson, S., Benn, D.I., Evans, D.J.A., Mitchell, W.A., 1996. The quaternary glacial history of the Lahul Himalaya, northern India. J. Quat. Sci. 11, 25–42.
Owen, L.A., Dortch, J.M., 2014. Nature and timing of Quaternary glaciation in the Himalayan–Tibetan orogen. Quat. Sci. Rev. 88, 14–54.
Owen, L.A., Gualtieri, L., Finkel, R.C., Caffee, M.W., Benn, D.I., Sharma, M.C., 2001. Cosmogenic radionuclide dating of glacial landforms in the Lahul Himalaya, northern India: defining the timing of Late Quaternary glaciation. J. Quat. Sci. 16, 555–563.
Owen, L.A., Mitchell, W., Bailey, R.M., Coxon, P., Rhodes, E., 1997. Style and timing of Glaciation in the Lahul Himalaya, northern India: a framework for reconstructing late Quaternary palaeoclimatic change in the western Himalayas. J. Quat. Sci. 12, 83–109.
Phadtare, N.R., 2000. Sharp decrease in summer monsoon strength 4000–3500 cal yr B.P. In the central higher Himalaya of India based on pollen evidence from alpine peat. Quat. Res. (Duluth) 129, 122–129.
Porter, S.C., 1970. Quaternary glacial record in swat kohistan. West Pakistan. Geol. Soc. Am. Bull. 81, 1421–1446.
Putkonen, J., O'Neal, M., 2006. Degradation of unconsolidated Quaternary landforms in the western North America. Geomorphology 75, 408–419.
Putkonen, J., Swanson, T., 2003. Accuracy of cosmogenic ages for moraines. Quat. Res. (Duluth) 59, 255–261.
Putkonen, J., Connolly, J., Orloff, T., 2008. Landscape evolution degrades the geologic signature of past glaciations. Geomorphology 97, 208–217.
Putnam, A.E., Schaefer, J.M., Denton, G.H., Barrell, D.J.A., Andersen, B.G., Koffman, T.N.B., Rowan, A.V., Finkel, R.C., Rood, D.H., Schwartz, R., Vandergoes, M.J., Plummer, M.A., Brocklehurst, S.H., Kelley, S.E., Ladig, K.L., 2013a. Warming and glacier recession in the rakaia valley, southern Alps of New Zealand, during heinrich stadial 1. Earth Planet Sci. Lett. 382, 98–110.
Putnam, A.E., Schaefer, J.M., Denton, G.H., Barrell, D.J.A., Birkel, S.D., Andersen, B.G., Kaplan, M.R., Finkel, R.C., Schwartz, R., Doughty, A.M., 2013b. The last glacial maximum at 44°S documented by a ^{10}Be moraine chronology at lake ohau, southern Alps of New Zealand. Quat. Sci. Rev. 62, 114–141.
Rawat, S., Gupta, A.K., Sangode, S.J., Srivastava, P., Nainwal, H.C., 2015a. Late pleistocene-holocene vegetation and indian summer monsoon record from the lahaul, northwest Himalaya, India. Quat. Sci. Rev. 114, 167–181.
Rawat, S., Gupta, A.K., Srivastava, P., Sangode, S.J., Nainwal, H.C., 2015b. A 13,000 year record of environmental magnetic variations in the lake and peat deposits from the Chandra valley, Lahaul: implications to Holocene monsoonal variability in the NW Himalaya. Palaeogeogr. Palaeoclimatol. Palaeoecol. 440, 116–127.
Roe, G.H., 2011. What do glaciers tell us about climate variability and climate change? J. Glaciol. 57, 567–578.
Roe, G.H., O'Neal, M.A., 2009. The response of glaciers to intrinsic climate variability: observations and models of late-Holocene variations in the Pacific Northwest. J. Glaciol. 55, 839–854.
Röhringer, I., Zech, R., Abramowski, U., Sosin, P., Aldahan, A., Kubik, P.W., Zöller, L., Zech, W., 2012. The late Pleistocene glaciation in the Bogchigir Valleys (Pamir, Tajikistan) based on ^{10}Be surface exposure dating. Quat. Res. (Duluth) 78, 590–597.
Rowan, A.V., 2016. The 'Little Ice Age in the Himalaya: a review of glacier advance driven by Northern Hemisphere temperature change. Holocene 1–17.
Rupper, S., Roe, G., 2008. Glacier changes and regional climate: a mass and energy balance approach. J. Clim. 21, 5384–5401.
Rupper, S., Roe, G., Gillespie, A., 2009. Spatial patterns of Holocene glacier advance and retreat in Central Asia. Quat. Res. (Duluth) 72, 337–346.
Sachs, J.P., Sachse, D., Smittenberg, R.H., Zhang, Z., Battisti, D.S., Golubic, S., 2009. Southward movement of the Pacific intertropical convergence zone AD 1400–1850. Nat. Geosci. 2, 519–525.
Saha, S., Sharma, M.C., Murari, M.K., Owen, L.A., Caffee, M.W., 2016. Geomorphology, sedimentology and minimum exposure ages of streamlined subglacial landforms in the NW Himalaya, India 2016. Boreas 45, 284–303.
Scherler, D., Bookhagen, B., Strecker, M.R., 2011. Hillslope-glacier coupling: the interplay of topography and glacial dynamics in High Asia. J. Geophys. Res.

Earth Surf 116, 1–21.
Schimmelpfennig, I., Schaefer, J.M., Akçar, N., Ivy-Ochs, S., Finkel, R.C., Schlüchter, C., 2012. Holocene glacier culminations in the Western Alps and their hemispheric relevance. Geology 40, 891–894.
Schimmelpfennig, I., Schaefer, J.M., Akçar, N., Koffman, T., Ivy-Ochs, S., Schwartz, R., Finkel, R.C., Zimmerman, S., Schlüchter, C., 2014. A chronology of Holocene and Little Ice Age glacier culminations of the Steingletscher, Central Alps, Switzerland, based on high-sensitivity beryllium-10 moraine dating. Earth Planet Sci. Lett. 393, 220–230.
Schindelwig, I., Akçar, N., Kubik, P.W., Schlüchter, C., 2012. Lateglacial and early Holocene dynamics of adjacent valley glaciers in the Western Swiss Alps. J. Quat. Sci. 27, 114–124.
Schlup, M., Carter, A., Cosca, M., Steck, A., 2003. Exhumation history of eastern Ladakh revealed by Ar-40/Ar-39 and fission-track ages: the Indus River-Tso Morari transect, NW Himalaya. Jgsl 160, 385–399.
Searle, M.P., Windley, B.F., Coward, M.P., Cooper, D.J.W., Rex, A.J., Rex, D., Tingdong, L., Xuchang, X., Jan, M.Q., Thakur, V.C., Kumar, S., 1987. The closing of Tethys and the tectonics of the Himalaya. Geol. Soc. Am. Bull. 98, 678–701.
Seong, Y.B., Owen, L.A., Bishop, M.P., Bush, A., Clendon, P., Copland, L., Finkel, R., Kamp, U., Shroder, J.F., 2007. Quaternary glacial history of the central Karakoram. Quat. Sci. Rev. 26, 3384–3405.
Seong, Y.B., Owen, L.A., Yi, C., Finkel, R.C., 2009. Quaternary glaciation of Muztag Ata and kongur Shan: evidence for glacier response to rapid climate changes throughout the late glacial and Holocene in westernmost Tibet. GSA Bulletin 121, 348–365.
Severinghaus, J.P., Beaudette, R., Headly, M.A., Taylor, K., Brook, E.J., 2009. The terrestrial biosphere. Science 324, 1431–1434.
Sharma, M.C., Owen, L.A., 1996. Quaternary glacial history of NW garhwal, central himalayas. Quat. Sci. Rev. 15, 335–365.
Sharma, P., Bourgeois, M., Elmore, D., Granger, D., Lipschutz, M.E., Ma, X., Miller, T., Mueller, K., Rickey, F., Simms, P., Vogt, S., 2000. PRIME lab AMS performance, upgrades and research applications. Nucl. Instruments Methods Phys. Res. Sect. B-Beam Interact. with Mater. Atoms 172, 112–123.
Sharma, S., Chand, P., Bisht, P., Shukla, A.D., Bartarya, S.K., Sundriyal, Y.P., Juyal, N., 2016. Factors responsible for driving the glaciation in the Sarchu plain, eastern zanskar Himalaya, during the late quaternary. J. Quat. Sci. 31, 495–511.
Shukla, S.P., Mishra, R., Chitranshi, A., 2015. Dynamics of Hamtah glacier, Lahul & spiti district, Himachal Pradesh. J. Ind. Geophys. Union 19, 414–421.
Solomina, O.N., Bradley, R.S., Hodgson, D.A., Ivy-Ochs, S., Jomelli, V., Mackintosh, A.N., Nesje, A., Owen, L.A., Wanner, H., Wiles, G.C., Young, N.E., 2015. Holocene glacier fluctuations. Quat. Sci. Rev. 111, 9–34.
Solomina, O.N., Bradley, R.S., Jomelli, V., Geirsdottir, A., Kaufman, D.S., Koch, J., McKay, N.P., Masiokas, M., Miller, G., Nesje, A., Nicolussi, K., Owen, L.A., Putnam, A.E., Wanner, H., Wiles, G., Yang, B., 2016. Glacier fluctuations during the past 2000 years. Quat. Sci. Rev. 149, 61–90.
Spicer, Robert A., 2017. Tibet, the Himalaya, Asian monsoons and biodiversity – in what ways are they related? Plant Diversity 39, 233–244.
Srivastava, P., Agnihotri, R., Sharma, D., Meena, N., Sundriyal, Y.P., Saxena, A., Bhushan, R., Sawlani, R., Banerji, U.S., Sharma, C., Bisht, P., Rana, N., Jayangondaperumal, R., 2017. 8000-year monsoonal record from Himalaya revealing reinforcement of tropical and global climate systems since mid-Holocene. Sci. Rep. 7, 1–10.
Steck, A., Epard, J.L., Vannay, J.C., Hunziker, J., Girard, M., Morard, A., Robyr, M., 1998. Geological transect across the Tso morari and spiti areas: the nappe structures of the tethys Himalaya. Eclogae Geologicae Helveticae 91, 103–121.
Stone, J.O., 2000. Air pressure and cosmogenic isotope production. J. Geophys. Res. 105, 23,753–23,759.
Stutz, E., Thöni, L.M., 1987. The lower Paleozoic Nyimaling x granite in the Indian Himalaya (Ladakh): new Rb/Sr data versus zircon typology. Geol. Rundsch. 76, 307–315.
Su, Z., Shi, Y., 2002. Response of monsoonal temperate glaciers to global warming since the Little Ice Age. Quat. Bar Int. 97–98, 123–131.
Sugden, D.E., John, B.S., 1976. Glaciers and Landscape. Edward Arnold, London.
Taylor, J.R., 1997. An Introduction to Error Analysis, second ed. University Science Books, Sausalito, CA.
Taylor, P.J., Mitchell, W.A., 2000. The quaternary glacial history of the zanskar range, north-west indian Himalaya. Quat. Int. 65/66, 81–99.
Thompson, L.G., Mosley-thompson, E., Davis, M.E., Lin, P., Henderson, K., Mashiotta, T.A., 2003. Tropical glacier and ice core evidence of climate change on annual to millennial time scales. Climatic Change 59, 137–155.
Thompson, L.G., Tao, T., Davis, M.E., Henderson, A., Mosley-Thompson, E., Lin, P.N., Beer, J., Synal, H.A., Cole-Dai, J., Bolzan, J.F., 1997. Tropical climate instability: the last glacial cycle from a Qinghai- Tibetan ice core. Science (Wash. D C) 276, 1821–1825.
Uppala, S.M., KÅllberg, P.W., Simmons, A.J., Andrae, U., Bechtold, V.D.C., Fiorino, M., Gibson, J.K., Haseler, J., Hernandez, A., Kelly, G.A., Li, X., Onogi, K., Saarinen, S., Sokka, N., Allan, R.P., Andersson, E., Arpe, K., Balmaseda, M.A., Beljaars, A.C.M., Van De Berg, L., Bidlot, J., Bormann, N., Caires, S., Chevallier, F., Dethof, A., Dragosavac, M., Fisher, M., Fuentes, M., Hagemann, S., Hólm, E., Hoskins, B.J., Isaksen, L., Janssen, P.A.E.M., Jenne, R., Mcnally, A.P., Mahfouf, J.F., Morcrette, J.J., Rayner, N.A., Saunders, R.W., Simon, P., Sterl, A., Trenberth, K.E., Untch, A., Vasiljevic, D., Viterbo, P., Woollen, J., 2005. The ERA-40 re-analysis. Q. J. R. Meteorol. Soc. 131, 2961–3012.
van der Bilt, W.G.M., Bakke, J., Vasskog, K., D'Andrea, W.J., Bradley, R.S., Ólafsdóttir, S., 2015. Reconstruction of glacier variability from lake sediments reveals dynamic Holocene climate in Svalbard. Quat. Sci. Rev. 126, 201–218.
Vermeesch, P., 2009. RadialPlotter: a Java application for fission track, luminescence and other radial plots. Radiat. Meas. 44, 409–410.
von Rad, U., Schaaf, M., Michels, K.H., Schulz, H., Berger, W.H., Sirocko, F., 1999. A 5000-yr record of climate change in varved sediments from the oxygen minimum zone off Pakistan, northeastern Arabian Sea. Quat. Res. (Duluth) 51, 39–53.
Wang, X., Auler, A.S., Edwards, R.L., Cheng, H., Cristalli, P.S., Smart, P.L., Richards, D.A., Shen, C.C., 2004. Wet periods in northeastern Brazil over the past 210 kyr linked to distant climate anomalies. Nature 432, 740–743.
Wang, Y., Cheng, H., Edwards, R.L., He, Y., Kong, X., An, Z., Wu, J., Kelly, M.J., Dykoski, C.A., Li, X., 2005. The Holocene asian monsoon: links to solar changes and north atlantic climate. Science 308, 854–858.
Wang, Y.J., Cheng, H., Edwards, R.L., An, Z.S., Wu, J.Y., Shen, C.C., Dorale, J.A., 2001. A high-resolution absolute-dated late Pleistocene Monsoon record from Hulu Cave, China. Science 294, 2345–2348.
Wanner, H., Mercolli, L., Grosjean, M., Ritz, S.P., 2015. Holocene climate variability and change: a data-based review. J. Geol. Soc. London 172, 254–263.
Ward, D.J., Anderson, R.S., 2011. The use of ablation-dominated medial moraines as samplers for 10Be-derived erosion rates of glacier valley walls, Kichatna Mountains, AK. Earth Surf. Process. Landforms 36, 495–512.
Ward, D.J., Anderson, R.S., Guido, Z.S., Briner, J.P., 2009. Numerical modeling of cosmogenic deglaciation records, Front Range and San Juan mountains, Colorado. J. Geophys. Res. Earth Surf 114.
Ward, D.J., Cesta, J.M., Galewsky, J., Sagredo, E., 2015. Late pleistocene glaciations of the arid subtropical Andes and new results from the Chajnantor Plateau, northern Chile. Quat. Sci. Rev. 128, 98–116.
Warren, C.R., Hulton, N.R.J., 1990. Topographic and glaciological controls on Holocene ice-sheet margin dynamics, central west Greenland. Ann. Glaciol. 14, 307–310.
Wünnemann, B., Demske, D., Tarasov, P., Kotlia, B.S., Reinhardt, C., Bloemendal, J., Diekmann, B., Hartmann, K., Krois, J., Riedel, F., 2010. Hydrological evolution during the last 15kyr in the Tso Kar lake basin (Ladakh, India), derived from geomorphological, sedimentological and palynological records. Quat. Sci. Rev. 29, 1138–1155.
Yancheva, G., Nowaczyk, N.R., Mingram, J., Dulski, P., Schettler, G., Liu, J., Sigman, D.M., Peterson, L.C., Haug, G.H., 2007. Influence of the intertropical convergence zone on the East Asian monsoon. Nature 445, 3–6.
Yanhong, W., Lücke, A., Zhangdong, J., Sumin, W., Schleser, G.H., Battarbee, R.W., Weilan, X., 2006. Holocene climate development on the central Tibetan Plateau: a sedimentary record from Cuoe Lake. Palaeogeogr. Palaeoclimatol. Palaeoecol. 234, 328–340.
Young, N.E., Briner, J.P., Rood, D.H., Finkel, R.C., 2012. glacier extent during the younger Dryas and 8.2-ka event on baffin island, arctic Canada. Science 80 (337), 1330–1333.
Yu, Y., Yang, T., Li, J., Liu, J., An, C., Liu, X., Fan, Z., Lu, Z., Li, Y., Su, X., 2006. Millennial-scale Holocene climate variability in the NW China drylands and links to the tropical Pacific and the North Atlantic. Palaeogeogr. Palaeoclimatol. Palaeoecol. 233, 149–162.
Zhang, C., Mischke, S., 2009. A Lateglacial and Holocene lake record from the Nianbaoyeze Mountains and inferences of lake, glacier and climate evolution on the eastern Tibetan Plateau. Quat. Sci. Rev. 28, 1970–1983.
Zhou, S., Li, J., Zhao, J., Wang, J., Zheng, J., 2011. Quaternary glaciations. Extent and chronology in China. Dev. Quat. Sci. 15, 981–1002.
Zhu, L., Zhen, X., Wang, J., Lü, H., Xie, M., Kitagawa, H., Possnert, G., 2009. A ~30,000-year record of environmental changes inferred from Lake Chen Co, Southern Tibet. J. Paleolimnol. 42, 343–358.